Chapter 4
Recent Trends in the Processing and Applications of Carbon Nanotubes and C-MEMS-Based Carbon Nanowires

Bidhan Pramanick, Merin Mary Meyn, Kavita Shrivastava, Sergio O. Martinez-Chapa and Marc J. Madou

Abstract In this chapter, we review the processing of carbon nanotubes from the first reported work to the present and cover a myriad of CNT applications. For CNT processing, the three most used techniques, i.e., arc discharge, laser ablation, and chemical vapor deposition for both multiwall and single-wall CNTs are detailed. We will learn that these fabrication techniques often need to be adapted to serve a specific application. We analyze processing techniques for CNT application in gas sensors, biosensors, optical sensors, supercapacitors, micro-/nanoelectronics, and in nano-electromechanical systems. Since the poor adhesion between CNTs and substrates often limits their application, we also survey the work of researchers who developed surface modification techniques. Although CNT research is quite a mature field, it still faces major challenges, including making ohmic contacts, selecting for a precise tube diameter and a precise tube length as well as problems with nanotube positioning accuracy. This explains why the large-scale manufacture of CNT devices remains a daunting task. Due to these limitations in the use of CNTs in a manufacturing environment, we propose an alternative, i.e., C-MEMS or carbon-MEMS.

B. Pramanick (✉) · S.O. Martinez-Chapa · M.J. Madou
School of Engineering and Sciences, Tecnologico de Monterrey,
64849 Mexico, N.L, Mexico
e-mail: bidhan.pramanick@gmail.com

S.O. Martinez-Chapa
e-mail: smart@itesm.mx

M.M. Meyn · K. Shrivastava
Avionics, IIST Valiamala, Thiruvananthapuram 695547, Kerala, India
e-mail: merinmeyn@gmail.com

K. Shrivastava
e-mail: kavitashrivastava998@gmail.com

M.J. Madou
Department of Mechanical and Aerospace Engineering, UC Irvine
CA 92697-3975, USA
e-mail: mmadou@uci.edu

Z.H. Khan (ed.), *Nanomaterials and Their Applications*,
Advanced Structured Materials 84, https://doi.org/10.1007/978-981-10-6214-8_4

A common C-MEMS fabrication process starts with photolithography of a high-carbon content photosensitive polymer precursor and it is followed by carbonization, also called pyrolysis, of the patterned polymer. Carbon nanowires (CNWs), fabricated by electrospinning of suspended polymer nanowires and photolithography of the contact pads for the suspended wires to attach too and the subsequent pyrolysis of this hybrid construct, have the potential of alleviating some of the aforementioned problems with CNTs. We review the C-MEMS fabrication process of CNWs in detail, compare their properties with CNTs, and discuss their various applications in this chapter.

Keywords CNT · Arc discharge · Laser ablation · Chemical vapor deposition C-MEMS · CNW · Electrospinning · EMS

4.1 Introduction

Carbon-based micro- or nanostructures are the strongest in nature because of the strength of the carbon–carbon chemical bond and crystallinity that is maintained even down to the molecular scale of a benzene ring. Carbon nanotubes (CNTs), one of the allotropes of carbon, have, compared to diamond, graphite, glassy carbon, buckyballs, and amorphous carbon, the highest electrical and thermal conductivity and are also the strongest and stiffest allotrope to be discovered so far. Thus, CNTs are the obvious choice for fundamental research as well as nanoelectronics and nanoelectromechanical (NEMS) applications. The large surface-to-volume ratios of these one-dimensional structures also make them ideal candidates to solve problems in the sensing arena and heat management say in modern computer systems.

Carbon nanotubes (CNTs) can be envisioned as tiny cylinders composed of rolled-up graphite planes with sp2 hybridized carbon. They come with a length-to-diameter ratio greater than 1,000,000. CNTs were first reported by Sumio lijima in 1991 when he fabricated this carbon allotrope using the arc discharge process [1]. These CNTs are a form of crystalline carbon with extraordinary mechanical, chemical, physical, and electrical properties. They may be single-walled CNTs (SWCNTs), multiwalled CNTs (MWCNTs) or come in the form of ropes composed of arrays of CNTs, depending on how they are produced and processed. There is a wide range of applications of CNTs in electronics, polymers (e.g., as additives), structural materials, energy storage, optics, and sensing to name a few. An often touted application, exploiting the high mechanical strength of CNTs, is their proposed use for the cabling of a space elevator, a concept introduced in the late nineteenth century that allows vehicle transport from the earth surface into space [2]. Heat dissipation is becoming an increasingly crucial problem in modern-day electronic devices and among the various polymers and nanometric materials used for thermal management purposes, CNTs have attracted extensive attention due to their ultrahigh thermal conductivity; about 600–3000 W/(m K) for an individual MWCNT. CNT research still faces challenges, including

making ohmic contacts, selecting for a precise tube diameter and a precise tube length as well as problems with nanotube positioning accuracy. Therefore, we propose an alternative, i.e., carbon-MEMS or C-MEMS.

In the past 15 years, C-MEMS has received a lot of attention because of the simple and inexpensive fabrication steps that are involved. Generally, a C-MEMS fabrication process starts with photolithography of a photosensitive polymer precursor and it is followed by pyrolysis, of the patterned polymer. Carbon nanowire (CNW) devices, fabricated by photolithography of the contact pads, electrospinning of suspended polymer nanowires, and the subsequent pyrolysis of this hybrid construct, have the potential of alleviating some of the aforementioned problems with CNTs. In the process just described, the ohmic contacts between the CNWs and the suspending electrodes are automatically established during carbon–carbon bond formation in the pyrolysis process. The length of the wires is fixed by the distance between the suspending electrodes and the CNW diameter is set by the electrospinning and carbonization process parameters. Suspending the CNWs between carbon electrodes solves the problem of surface interference and makes for better sensor and electronic component performance. The smaller the diameter of the CNWs the more graphitic the microstructure with a resultant higher conductivity and higher Young's modulus (e.g., for a 200 nm CNW, Young's modulus is 350 GPa vs. 1 TPa for a SWCNT) [2]. Although the properties of the suspended CNWs are not comparable yet to those of CNTs, they get better and better as the wire diameter is further decreased. Most importantly, using a variant of electrospinning for writing the polymer precursor pattern, i.e., electromechanical spinning (EMS), we can write CNW networks with an exact control over position, ohmic contacts, length, and diameter of the CNWs.

4.2 CNT Processings

The first reported CNTs, fabricated by Sumio lijima, are shown in Fig. 4.1 [1]. In each tube, the carbon-atom hexagons are arranged in helical fashion about the tube axis. In this section, we will discuss about the most common processing methods of CNTs, which are classified as electric arc discharge, laser ablation, and chemical vapor deposition (CVD).

In the electric arc discharge method, a voltage of 20–25 V is applied between two graphite electrodes resulting in a DC current of 50–120 A and growth of CNTs. This method can easily produce straight and near perfect MWCNTs. Using a carbon anode packed with catalyst, isolated or bundled SWCNTs can also be grown in the discharge chamber by covaporization of graphite and catalyst.

In the laser ablation technique, a pulsed laser vaporizes a composite target of graphite and catalyst resulting in the high yields of SWCNTs. When only a graphite target is used, the resultant homogeneous carbon vapor condenses into capped MWCNTs. Compared with MWCNTs prepared in an arc discharge chamber, the MWCNTs grown in a laser ablation process are relatively short.

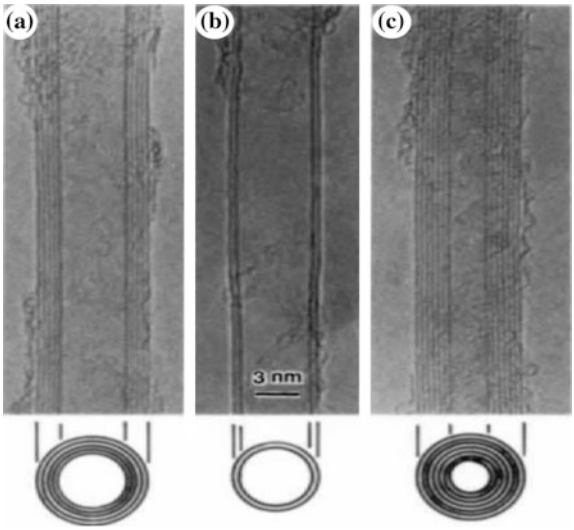

Fig. 4.1 Electron micrographs of first reported CNTs [1]

CVD is a process in which gaseous molecules, called precursors, are transformed into solid materials on a substrate via chemical reactions. For producing CNTs, a hydrocarbon vapor, such as methane, ethylene, acetylene, xylene, benzene, or toluene, is used as the precursor. Unlike the arc discharge method and the laser ablation technique, catalysts are needed in a CVD process. Low-temperature growth of CNTs is possible in CVD when a plasma source is used, called plasma-enhanced CVD (PECVD). The CVD-grown CNTs usually show poor crystallinity and a post-synthesis high-temperature treatment is often used to improve the product quality.

Various research groups have used different precursors for the above-mentioned techniques, and they also have modified the general procedures. In the following subsection, we will report few of the research works on CNT fabrication for each of the three techniques previously introduced.

4.2.1 Arc Discharge Method

In Fig. 4.2, we show a diagram of the arc discharge apparatus used by Kim et al. [2]. Pure graphite (purity of 99.999%) anodes and cathodes were used where the gap between the electrodes was maintained constant at 0.5–2 mm by advancing the consumed anode toward the cathode. A carbon plasma was generated at various currents (10–70 A) and voltages of 18–30 V and at chamber pressure of approximately 30–500 Torr. The chamber and carbon cathode were cooled by a cold water line. The catalyst, ferrocene, was introduced into the furnace by a carrying gas, and the temperature of xylene–ferrocene mixture in the jar was kept at 80 °C by using

an oil bath [2]. It was found that both SWCNT and MWCNT were obtained by this method: MWNTs are observed in the samples collected in the central area of the cathode (Fig. 4.3a) and SWNTs were detected in the flake samples collected around the cathode, and cooling water line (Fig. 4.3b).

The formation of single-walled CNTs by DC arc discharge is reported by Sato et al. [3]. CNTs form when carbon and metal are mixed in the gaseous phase after vaporization and are cooled together into liquid droplets as saturated carbon form SWCNTs during cooling precipitation. The mass synthesis of SWCNTs depends on the amount of liquid droplets formed. Carbon-saturated-metal liquid droplets form in the local thermal equilibrium of plasma, by collision between charged particles at high temperature. For the fabrication of SWCNTs using DC arc discharge, Sato et al. found that high-efficiency of graphitization catalysts, low solubility in carbon, self-assembly of metal, and growth temperature of SWCNTs were all important factors. The precipitation of carbon atoms from their saturated state in the liquid droplets leads to SWCNT growth during cooling and that growth depends on the nature of the catalyst governing both sublimation and solidification temperatures.

Researchers have tried many modifications of the arc discharge process to increase the CNTs yield and quality, and to control the CNT dimensions (diameter, length, purity). In a study, reported by Kanai et al. [4], the fabrication of CNTs is carried out in a gravity-free (0G) arc discharge and an increased yield of SWNTs was demonstrated. In a gravity-free arc discharge process, the convective flow of buffer gas during the arc discharge is reduced, which results in an increase of the high thermostatic volume of the arc flame. The yield of both soot and SWNTs in soot was increased. The SWNT yield in soot under 0G conditions was $\sim$2.2 times larger than that under 1G. In both cases, arc discharge conditions such as arc current, arc gap, and the pressure of gas were maintained constant. The analysis made by Kanai et al. revealed that the diameter distribution of SWNTs was shifted to a larger diameter regime under gravity-free conditions. The annealing process in high thermostatic atmosphere was one of the important factors to selectively synthesize a certain diameter SWNT in high yield.

Keidar et al. [5] proposed synthesis of CNTs by magnetically enhanced arc discharge (MEAD). Obtaining better control over the different properties of

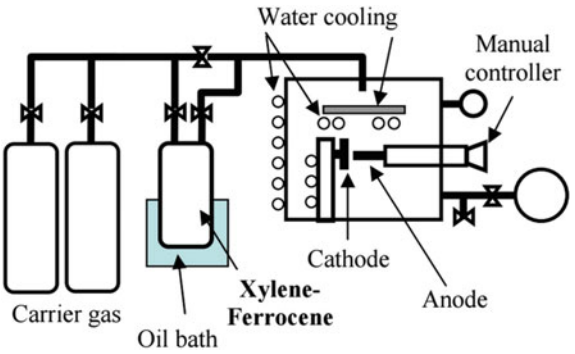

Fig. 4.2 Diagram of the arc discharge apparatus [2]

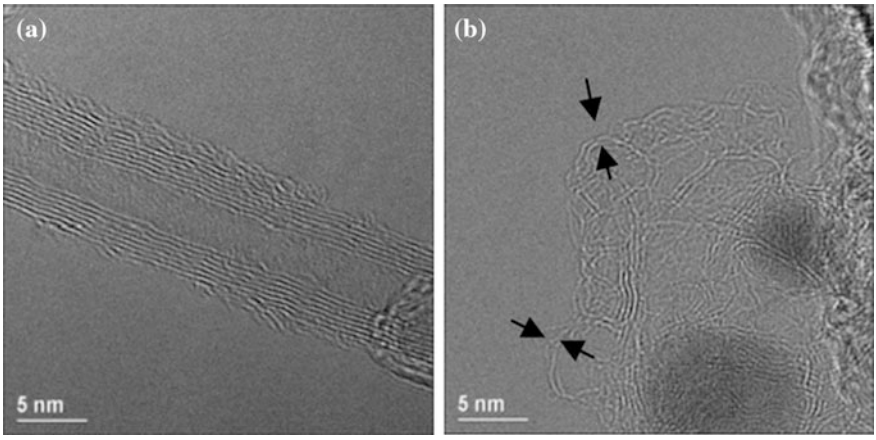

Fig. 4.3 TEM images of samples collected in **a** the central area of cathode and **b** around the cathode [2]

SWCNTs was an important objective during the production of SWCNTs. The application of a magnetic field produces higher plasma densities which lead to changes in the cathode and anode erosion rate. So the carbon deposit produced in MEAD is different from that without magnetic field. Both the length of the SWCNTs and the purity level of the carbon deposit were found to increase upon the application of a magnetic field at the time of the arc discharge. The carbon deposited by arc discharge, due to the magnetic field, mainly consists of isolated and bunched SWCNTs. In Fig. 4.4a, we show the MEAD setup, and in Fig. 4.4b, we show the schematic of an anodic arc discharge process. In Keidar et al.'s work, the interaction of CNTs and the growth phenomenon of CNTs in arc plasma were studied with an emphasis on such important effects like anode ablation that supplies the carbon plasma in an anodic arc discharge technique, and the momentum, charge, and energy transfer processes between nanotube and plasma. The length and charge density of CNTs depend on the plasma density and the electric field intensity in the electrode gap. The most important feature of CNTs produced by the arc discharge process is that they have very few structural defects compared to CNTs produced by other methods. These high-quality CNTs also exhibit a very low degradation of emissivity over time. The purity of the sample with the application of a magnetic field is also high compared to that of the conventional process because of some particular ratio between ion and neutral density may be optimal for the SWNT growth.

Sugai et al. [6] reported the fabrication of SWCNTs and fullerenes using high-temperature pulsed arc discharge. The pulse arc method for CNT production requires high temperature, long pulses, and noble inert gases like argon (Ar), helium (He), and krypton (Kr) as buffer gas. In Fig. 4.5, we show a schematic of the pulsed arc discharge used by Sugai et al. The apparatus consists of a furnace (ISUZU KRO-12K), a quartz tube, electric feedthroughs with insulation quartz tubes, carbon electrodes, a water-cooled trap, and their homemade pulsed HV power supply. The

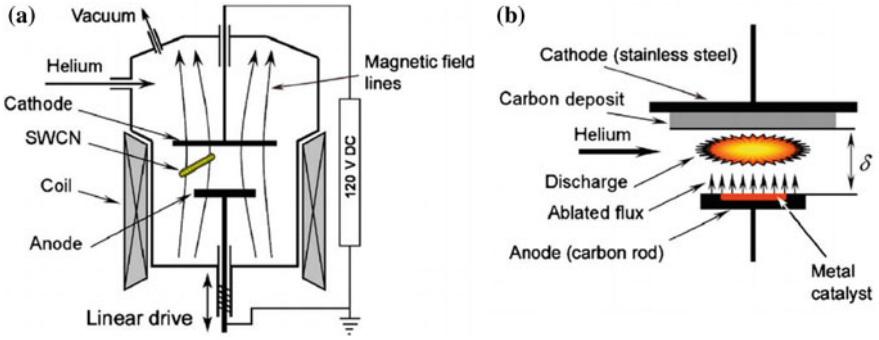

Fig. 4.4 **a** Setup of MEAD and **b** the schematic of the anodic arc discharge [5]

electrodes were located inside the quarts tube and the furnace to produce pulsed arc discharges in high-temperature buffer gases. In this method, metal-doped composite graphite rods (Ni/Co: 0.7/0.7 at. %, and Ni/Y 4.2/1.0 at. %; Toyo Tanso Co. Ltd) and pure graphite rods (Toyo Tanso Co. Ltd) were used as the electrodes. A buffer gas (He, Ar, or Kr) was passed through the quartz tube to thermally anneal carbon clusters and particles produced by the pulsed arc discharge. The temperature of the tube was varied between 25 and 1100 °C by the furnace. The fullerenes, SWNTs, and other graphitic particles drifted within the tube by the gas flow and were collected on the water-cooled copper trap. Fullerenes were identified by high-performance liquid crystal chromatography and transmission electron microscopy. Scanning electron microscopy analysis revealed the production of significant amount of SWCNTs in the carbon soot. The dependence of fullerene concentration on temperature, HV pulse duration, and buffer gas species was measured. The yield

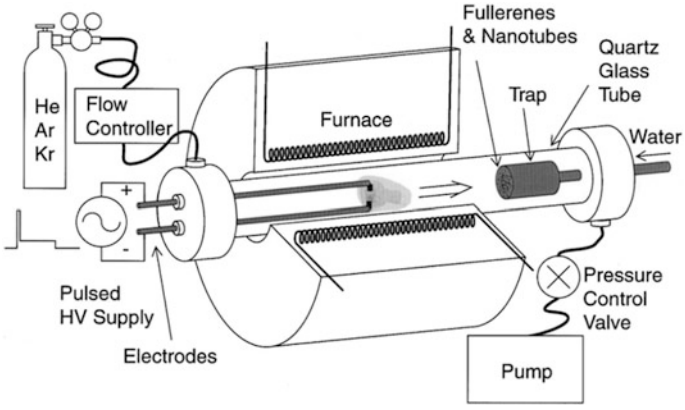

Fig. 4.5 Schematic of pulsed arc discharge [6]

Fig. 4.6 TEM image of single-wall nanotube [6]

of SWCNT production increased with an increase of pulse width duration, while the yield of fullerenes decreased when decreasing the pulse width. A TEM image of a single-wall nanotube is shown in Fig. 4.6.

Ando et al. report on the production of thick-walled CNTs by arc discharge in a hydrogen atmosphere [7]. Although SWNTs might possess very small diameter d ($0.7 < d < 2$ nm), for some applications, such as hydrogen storage and synthesis of fullerene-encapsulated SWNTs, thick SWNTs are advantageous. Ando et al. reported the preparation of thick SWNTs with diameters of 1.4–4 nm. The research group also described the growth mechanism of double-walled carbon nanotubes (DWNTs) coexisted with thick SWNTs. In the experimental setup, metal-doped carbon was used as the cathode and pure carbon was used as the anode and those electrodes were installed horizontally in the reactor. At a pressure of 60–700 Torr, a DC arc voltage was applied and the arc current was changed from 30 to 70 A. The chamber soot was collected and investigated by SEM equipped with an energy-dispersive X-ray analysis system (EDX), HR-TEM, and Raman spectroscopy. Using Fe (1 at.%) as catalyst, a large number of SWNTs were produced in H_2 gas and the yield of SWNTs in the chamber soot became higher with increasing H_2 gas pressure from 60 to 500 Torr and got saturated thereafter. However, SWNTs could not be prepared in pure H_2 gas using Co or Ni catalysts or their combination, unless 1% H_2S gas was added to the ambient.

4.2.2 Laser Ablation Method

Laser ablation method is a promising technique for producing SWCNTs and MWCNTs. This method for synthesizing CNTs was first reported by Guo et al. [8] in 1995. Schematic of their presented apparatus for laser ablation is shown in Fig. 4.7, which consists of a furnace, a quartz tube with a window, a target carbon

composite doped with catalytic metals, a water-cooled trap, and flow systems for the buffer gas to maintain constant pressures and flow rates. A laser beam (YAG or CO_2 laser) was introduced through the window and focused onto the target. The target was vaporized in high-temperature and forms SWNTs. The produced SWNTs were conveyed by the Ar buffer gas to the trap, cooled there, and collected. By this method, high-quality SWNT production, investigation of growth dynamics, and the production of new materials are done with diameter control of CNTs. The laser, having sufficiently high energy density, was capable to vaporize the target material at the molecular level.

Thess et al. [9] also produced the high-yield (>70%) SWNTs using this method by condensing laser-vaporized carbon–nickel–cobalt mixture at 1200 °C. They found that these SWNTs were nearly uniform in diameter and self-organized into ropes, forming two-dimensional triangular structures of 100–500 SWNTs.

The laser ablation method is also used to fabricate devices from separately grown SWCNTs. Chae et al. [10] reported on the concept of material-assisted laser ablation (MALA) for fabrication of SWCNTs. Single-walled carbon nanotubes were grown on quartz. Ferritin catalyst (Aldrich) diluted (1:20 by volume) with deionized water was cast onto the substrate. A high concentration of catalyst on a doublesided polished, quartz substrate was used to obtain a random network of tubes. The catalyst was oxidized in air by heating it up to 800 °C and cooling it back to room temperature. Heating to 925 °C in a 20 SCCM flow of hydrogen and 20 SCCM flow of argon, hydrogen bubbled through ethanol for 15 min producing random networks of individual single-walled tubes. After the growth, the samples were slowly cooled back to room temperature to prevent the quartz substrate from cracking. After the deposition of the target material, a photoablation assistor layer was coated on it. The Chae group used a conventional photoresist, MicroChem AZ4620 or MicroChem S1818, as the ablation assistor to coat the carbon nanotube

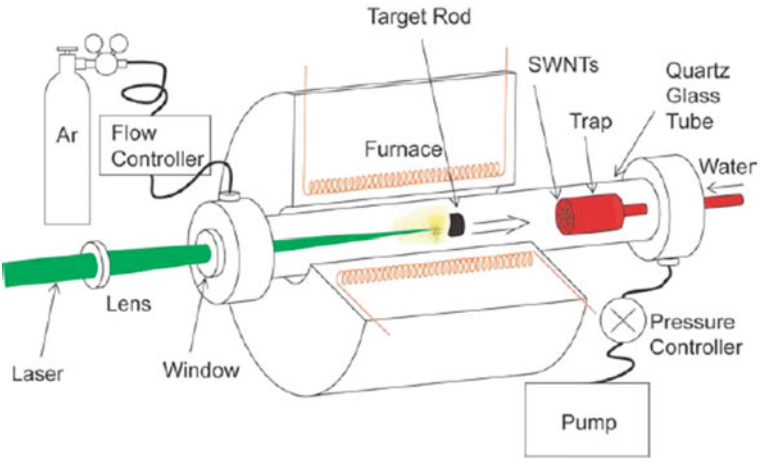

Fig. 4.7 Schematic diagram of laser-furnace apparatus [8]

layer. The concept of material-assisted excimer laser photoablation is shown in Fig. 4.8. Photoresist deposition process caused the resist to be placed under the carbon nanotubes as well as on top of the carbon nanotubes as the liquid-phase photoresist was coated and baked. After the coating of the photoablation assistor, it was ablated using pulsed excimer laser radiation (deep ultraviolet radiation from a KrF excimer laser at 248 nm wavelength). It was found that the carbon nanotube film can be patterned by the low-fluence photoablation process when a photoablation assistor is used, even though the fluence of illumination is lower than the threshold value for direct photoablation. However, the fabricated patterns were not clean as a residual layer remained after the process.

In a later work, Chae et al. found that the residue was formed because the carbon nanotubes were redeposited in the illuminated region where all of the polymer and carbon nanotubes were removed [11]. The concept of the MALA process and schematic illustration of Anvik large-area projection lithography and photoablation system are shown in Fig. 4.9a, b, respectively. Near the boundary of the patterns where some regions were illuminated and some were not, the residue layer was formed due to the exiting debris being attached to the polymer sidewalls. It was concluded that the residue layer at the edge of the pattern could be removed if a thinner polymer was used as the photoablation assistor, so that the ejected debris had a wider exiting angle from the substrate.

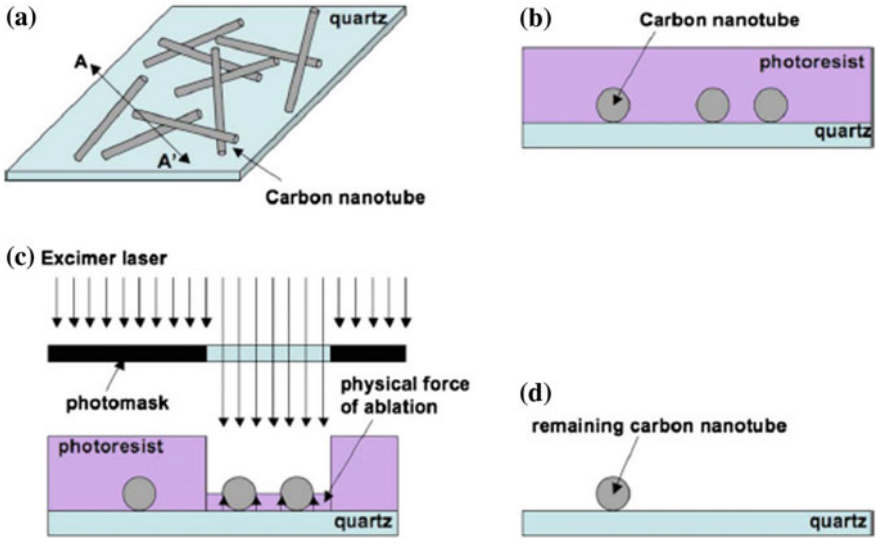

Fig. 4.8 Concept of material-assisted excimer laser photoablation. **a** Carbon nanotubes layer deposition on substrate, **b** photoablation assistor layer coating on the target material, the cross-sectional view of AA′ in **a** is illustrated, **c** ablation of the assistor layer and removal of the target material **d** patterned carbon nanotube film [10]

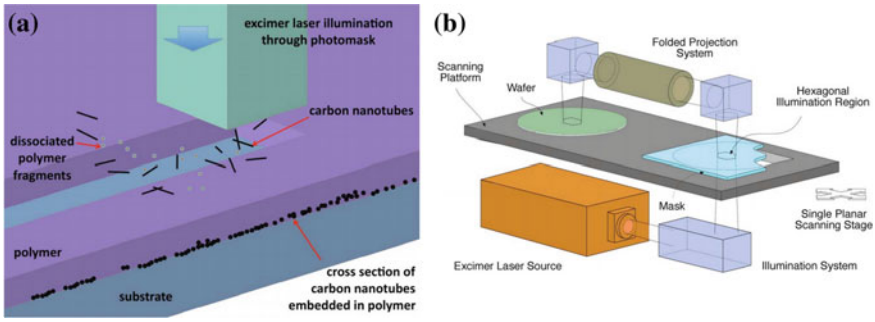

Fig. 4.9 **a** Concept of the MALA process and **b** schematic illustration of Anvik large-area projection lithography and photoablation system [11]

4.2.3 CVD Method

A method classified under CVD for the fabrication of vertically aligned CNT (VACNT) was reported by Wang et al. [12]. VACNT structure was fabricated by a thermal CVD process and metallization of Ti/Ni/Au was used to reduce the interfacial thermal resistance. The fabricated CNT structure was used as thermal interface material (TIM). Thermal conductivity achieved by this technique was about 250 W/(m. K) for bulk VACNT.

Horizontally aligned ultralong single-walled CNTs produced on silicon substrate were reported using fast-heating chemical vapor deposition by Nguyen et al. [13]. Ferric chloride ($FeCl_3$) and ethanol (C_2H_5OH) were used as catalyst and source of carbon, respectively. The fast heating of ethanol at the temperature of 900 °C for 60 min produced high-quality CNTs which were clean, ultralong, highly dense, and straight as parallel lines. The researchers did not find any CNTs on substrate at a growth temperature of 700 °C. Repeating the experiments for 800 °C, they found few CNTs, but not parallel.

The growth of a composite structure consisting of multilayered graphene which was supported by vertically aligned multiwalled CNT was reported by Matsuoka et al. [14]. The fabrication was done by chemical vapor deposition using ethanol as a source of carbon and iron layer as a catalyst. Thicker Fe films produced composite structures and thinner films produced pure vertically aligned multiwalled CNT. Medium thicknesses of Fe produced bundles of vertically aligned CNT fused together at the tip. Application of these types of composite structures includes efficient heat radiation and wiring for very large integrated circuits.

CVD growth of nanotubes, MWCNT, and graphene was affected by the thickness of catalyst film grown on the substrate. Extremely thin layer of catalyst resulted SWCNT, while thicker layer resulted MWCNT and extreme thick layer yielded graphene. For sufficiently thin film, it resulted in granulation of deposited metal film into the particles. Diameter of these particles defined the diameter of CNT and thus number of CNT walls. These particles were responsible for

significant increase in mobility, especially for metal atom near the film surface, allowing the metal film to lower its surface energy by granulation. For thick films, granulation did not occur under CVD conditions due to kinetic effect or due to lower thermodynamic driving force for granulation resulting from the smaller surface-to-volume ratio. Once the metal film was saturated with carbon, graphene formed on its surface. This process was self-limiting because the graphene prevented further carbon from reaching the catalyst (Fig. 4.10).

It is known that the yield and selectivity toward SWNTs, as well as the overall nanotube quality, depend on operating conditions (e.g., temperature, pressure, gas composition) and catalyst preparation parameters (e.g., type of metal used, total loading, addition of a second metal, type of support). Nguyen et al. reported the synthesis of single-walled carbon nanotubes over Co–Mo/Al_2O_3 catalyst by catalytic chemical vapor deposition of methane [15]. Alumina-supported Co–Mo samples prepared by the wet impregnation method were used as catalysts for the synthesis of SWNTs by CVD using CH_4 at 900 °C. The mass ratio of the bimetallic catalyst with a composition of Co: Mo: Al_2O_3 was demonstrated to play an important role in the formation of the SWCNTs obtained. The Co species mainly

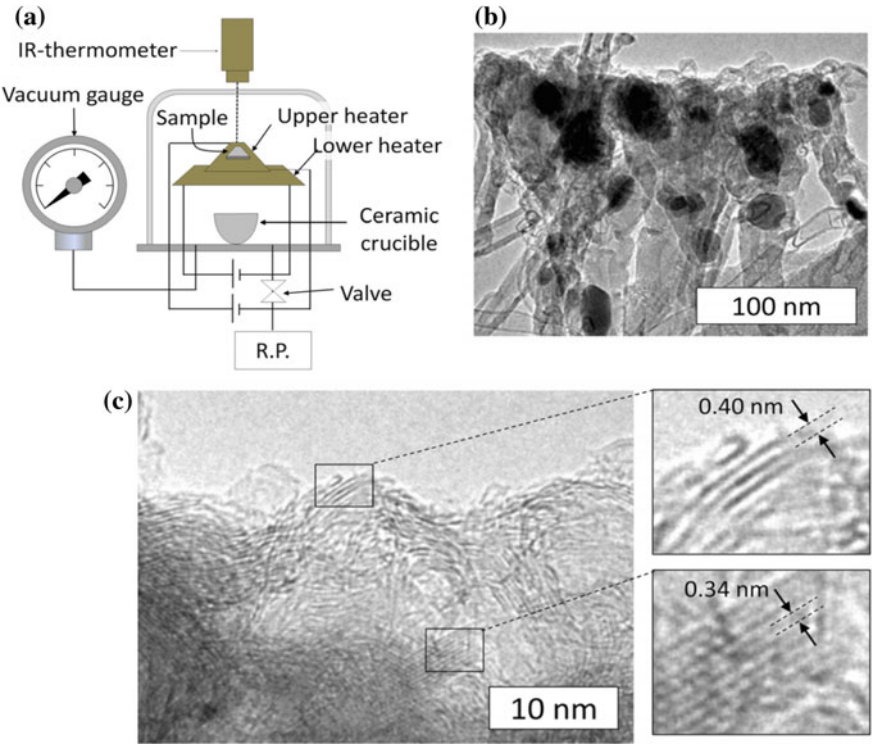

Fig. 4.10 **a** CVD apparatus for CNTs and composite synthesis, **b** TEM image of tip-bundled CNTs and **c** multilayer graphene near the surface of (**b**) [14]

generate the catalytic activity. However, with the increase of cobalt (II) nitrate hexahydrate content compared with that of ammonium heptamolubdate tetrahydrate, CNT density decreases. The diameter (d) was observed to be in the range of 0.76 to 1.69 nm. A TEM image of SWNT is shown in Fig. 4.11.

Synthesis of multiwalled CNT by radio frequency catalytic chemical vapor deposition (RF-CCVD) with bimetallic catalyst was also reported by Ramakrishnan et al. [16]. Highly pure crystalline multiwalled CNTs were synthesized by radio frequency catalytic chemical vapor deposition using acetylene as carbon source and also using bimetallic Fe–Co catalyst supported on CaO at 720 °C. Nanotubes of an average diameter of 14.7 ± 4.76 nm were produced. It was reported in the literature that induction heating is very useful for fabrication of high-quality CNT. The utilization of inductive heating in the synthesis of carbon nanotubes by CCVD significantly reduced the energy consumption, increased heating rate, and provided tighter control of the heating rate compared to external furnace methods.

Lee et al. [17] reported carbon nanotube fabrication by anodic aluminum oxide (AAO) nanotemplate. An AAO nanotemplate was deposited by two-step anodization method followed by deposition of Ni nanoparticles at bottom pore of template. Microwave plasma-enhanced CVD method was used for the growth of carbon nanotube on the template where Ni was used as catalyst and CH_4 as source of carbon. The range of diameter and density of AAO allowed using it as a microfilter template for growth of CNTs and metal or semiconductor nanowires. Planer and cross section of SEM images of CNTs are shown in Fig. 4.12a, b, respectively. AAO nanoporous templates with various pore sizes and depth were introduced to control the dimension and density of the CNTs arrays. They observed that anodization speed was dependent on voltage between anode and cathode. The grown CNTs were of 2 μm length and 50 nm diameter for the average diameter and interpore distance of 65 ± 7 nm and 82 ± 5 nm, respectively. The nanotemplate pore density and thickness were about 2.1×10^{10} pores/cm^2 and 1 μm, respectively.

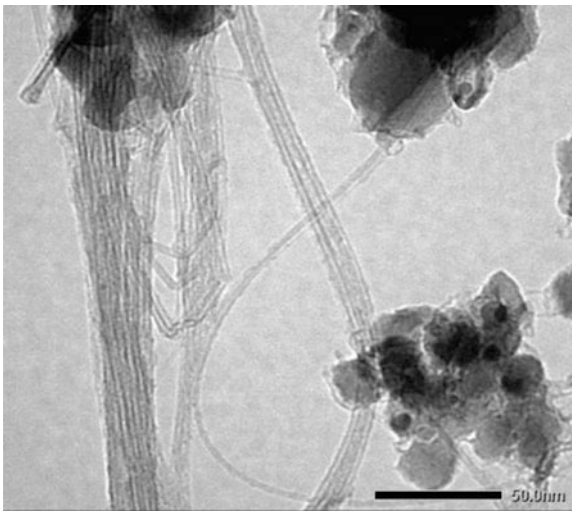

Fig. 4.11 TEM image of SWT grown onto Co–Mo/$A1_2O_3$ catalysts [15]

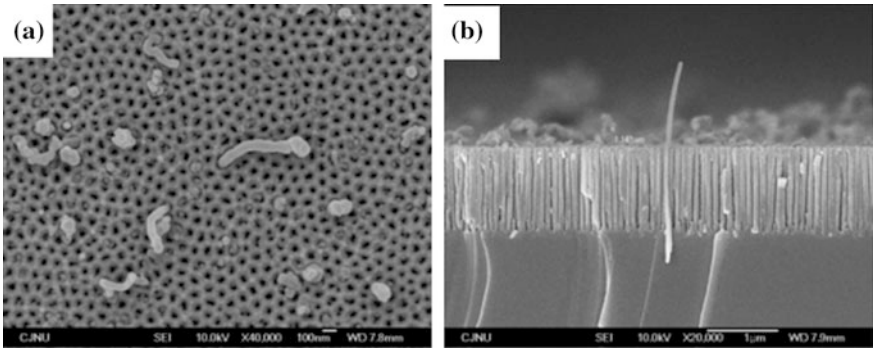

Fig. 4.12 **a** Planer and **b** cross section of SEM image of CNTs growth on AAO nanotemplate with Ni catalyst [17]

The effective methodology of combining focused ion beam and chemical vapor deposition is helpful for synthesis of carbon nanotube, triode-type multiwalled carbon nanotube and fabrication of single-walled carbon nanotube-based nanodevices. Vertically aligned CNTs show application for field emission and nanodevice interconnect. The decrease in width of interconnecting wire, usally aluminum or other metals, increases resistivity of wire which increases the delay. Therefore performance of the devices are affected. So vertically aligned CNTs are one of the replacements for this interconnecting wire. Horizontally aligned CNTs may be used as channel material between two electrodes of a FET; however, placement of CNTs is one of the challenges. Once the gate is fabricated, vertically aligned CNT can also be fabricated in each gate using plasma-enhanced chemical vapor deposition. Fabrication of vertical and horizontal CNTs using focused ion beam and chemical vapor deposition was reported in [18]. In a first step, metal-gated carbon nanotubes were fabricated on the multilayer substrate which contained a catalyst. In a second step, horizontally aligned single-walled carbon nanotubes were grown on the transmission electron microscopic grid. Bundled SWCNTs with a diameter of approximately 1–3 nm were obtained.

Wong et al. [19] reported the synthesis of multiwalled CNTs of uniform diameter using microwave plasma chemical vapor deposition method. Nitrogen (N_2) was used as carrier, and methane (CH_4) was used as carbon source. Thin iron films with different thicknesses, 0.5–5 nm, on silicon substrates acted as catalysts. Atomic force microscopy was used to investigate the relationship between the iron film thickness and the size of the iron clusters formed after the plasma treatment. Scanning and transmission electron microscopy were utilized to study the morphology, structure, and diameter of the as-grown CNTs. With the iron film thickness of 0.5 nm, the CNTs showed a remarkable structural uniformity in terms of diameter (standard deviation was 11.4% of the average diameter d).

Among all fabrication methods of CNT, plasma-enhanced chemical vapor deposition allows fabrication of different types of CNTs on a large area. This result

is difficult to be obtained on a large substrate using conventional microwave plasma source. On the other hand, if RF-excited plasma source is used with large electrodes, it has the drawback of occurrence of standing wave and skin effect which limit the plasma processing uniformity in large-area processes. A slot-excited microwave source produces CNT on plane surface of large size substrate as many slot antennas can be installed in a single waveguide and a number of waveguides can be arranged in parallel manner to produce plasma on large scale. The combination of this plasma production method and plasma-enhanced chemical vapor deposition technique of CNT gives good quality and larger area grown CNT. Fabrication of CNT by slot-excited microwave plasma-enhanced chemical vapor deposition (PECVD) was reported by Shim et al. [20]. A Schematic of experimental set up is shown in Fig. 4.13. Here plasma was produced by a slot antenna at 2.45 GHz microwave injection in CH_4/H_2 mixture. Quality of grown CNTs is controlled by optimization of one of the steps in catalyst treatment as preheating step.

A special processing technique for bulk production of CNTs was reported by Kim et al. [21] CNTs were produced in bulk by thermal induction plasma. A RF inductively coupled thermal plasma was employed to continuously synthesize SWCNT through the direct evaporation of a mixture of carbon black and metallic catalyst inside the plasma plume. The processing system consisted mainly of an RF plasma torch, which generates a plasma jet of extremely high temperature ($\sim$15,000 K), with a high energy density and abundance of reactive species (ions and neutrals). The Kim group did a parametric study which showed that the quality and purity of the SWNT produced are critically affected by the grade of carbon black, plasma gas composition, and metallic catalyst. In general, this process seems well suited for pushing SWCNT production to levels of hundreds of kilograms per year or higher.

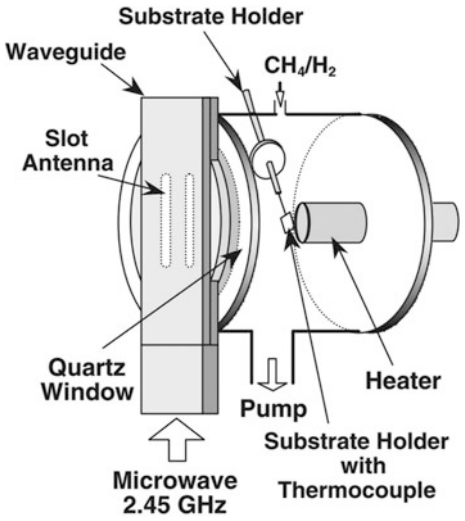

Fig. 4.13 Schematic of experimental setup [20]

4.3 Applications of CNTs

In this section, we analyze the processing techniques for various CNT applications including gas sensors, biosensors, optical sensors, supercapacitors, micro-/nanoelectronics, and nanoelectromechanical systems. Sometimes, the general techniques of CNTs processing are needed to be modified for actual applications. We will discuss in the following about the individual application and the modified fabrication technique if any used.

4.3.1 Gas Sensors

CNT-based gas sensors provide high sensitivity, low operating temperature, rapid response time, and selectivity to various gases. These sensors work on the principle of change in electrical properties caused by transfer of charges between gas molecules and CNT walls and some attached functional groups. CVD methods of fabrication are done at high temperatures and thus not within the temperature range sustainable by CMOS chips. A new low-temperature fabrication process based on "surface-programming assembly" was developed by Huang et al. [22]. Oxidized silicon surface modified to amino-terminated ($–NH_2$) self-assembled monolayer (SAM) with 3-aminopropyltriethoxysilane (APTS) was used as substrate. The substrates were cleaned with ethanol and acetone and dried with nitrogen. Then, these were soaked in the solution of APTS in acetone for 30 min to obtain amino-terminated SAM. The positive charges or amine groups cause adhesion of CNTs to the surface. The samples were cleaned again and the treatment resulted in complete coverage with APTS monolayer. By soaking in nanotube, suspended MWCNTs were deposited on the functionalized surface and samples were rinsed again. After CNTs adhered, interdigitated electrodes (IDE) were fabricated by depositing an Au layer on a SiO_2 surface and using conventional photolithography. Thus, array-type CNT-based gas sensors were developed and were tested for detection of CO and NH_3 at room temperatures. Schematic diagram of deposition of CNTs on the amino silanized SiO_2 surface and optical microscopic images of the CNT-based gas sensors are shown in Fig. 4.14a, b, respectively.

Quick and precise detection is required for highly inflammable and explosive hydrogen (H_2) gas. Metal oxide-based H_2 gas sensors have simple structure and low cost but operate at high temperatures consuming more power. Comparing pristine CNT-based gas sensors to the ones modified with acids, nanoparticles, and polymers, the former lack specificity and have low sensitivity. Dhall et al. used pristine MWCNTs (P-MWCNT) with purity >95% prepared by CVD method for functionalization process to attain increased sensitivity [23]. P-MWCNTs were heated at 400 °C to remove impurities and were dissolved in a mixture of sulfuric acid and nitric acid followed by sonication. The solution was kept at room temperature for 14 h, and then the acid was removed by centrifugation followed by washing in

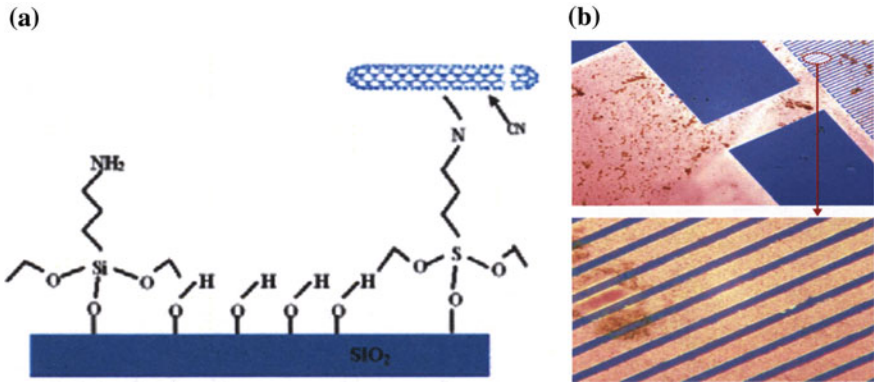

Fig. 4.14 **a** Schematic diagram of deposition of CNTs on the amino silanized SiO_2 surface and **b** Optical microscopic images of the CNT-based gas sensors [22]

deionized water. The P-MWCNTs were dried and again immersed in H_2O_2 for oxidation. In the next, H_2O_2 was removed by washing in deionized water. The functionalized MWCNTs (F-MWCNTs) were drop casted on the sensor which was fabricated on a Si/SiO_2. For the sensor fabrication, a Cr/Au layer was deposited by thermal evaporation and patterned by photolithography to get the desired patterns of interdigitated electrodes (IDEs). Solvent from the drop-casted F-MWCNTs was removed by heating the device, thereby resulting in a network of nanotubes in between electrodes. Schematic diagram of fabricated device and SEM image of fabricated interdigitated electrodes are shown in Fig. 4.15a, b, respectively. F-MWCNTs showed increased electrical conductivity and reduced crystallite size compared to P-MWCNTs. The electrical transport properties of F-MWCNTs increased to thousand times than P-MWCNTs due to the presence of functional groups that increases the number of bands close to the Fermi level, resulting in electron transfer between carbon atoms. Sensitivity of F-MWCNTs increased to 0.8% and recovery time decreases for the same concentration of H_2 gas when compared to responses of P-MWCNTs. Sensitivity of F-MWCNTs shows linear dependence of gas concentration while that of P-MWCNTs was independent of concentration. HR-TEM images of P-MWCNTs and F-MWCNTs are shown in Fig. 4.16a, b, respectively.

Yun et al. [24] reports an inkjet printing method of CNT gas sensor fabrication for massive production with reduced processing steps. SWCNTs of length shorter than 10 μm, synthesized by arc discharge, were dispersed in dimethylformamide (DMF) solution and centrifuged, and the supernatant was decanted for use in inkjet printing. A single-inkjet head equipped with a piezoelectric actuation module was used to eject SWCNT droplet on 4-in. silicon-on-insulator (SOI) wafer. Pt electrodes were patterned by e-beam evaporation followed by liftoff to remove the photoresist. SEM image of patterned CNT films under the Pt electrode and dried CNT by dropping between electrode fingers are shown in Fig. 4.17a, b, respectively. CNT droplets were observed distinctly on the finger electrode with precise

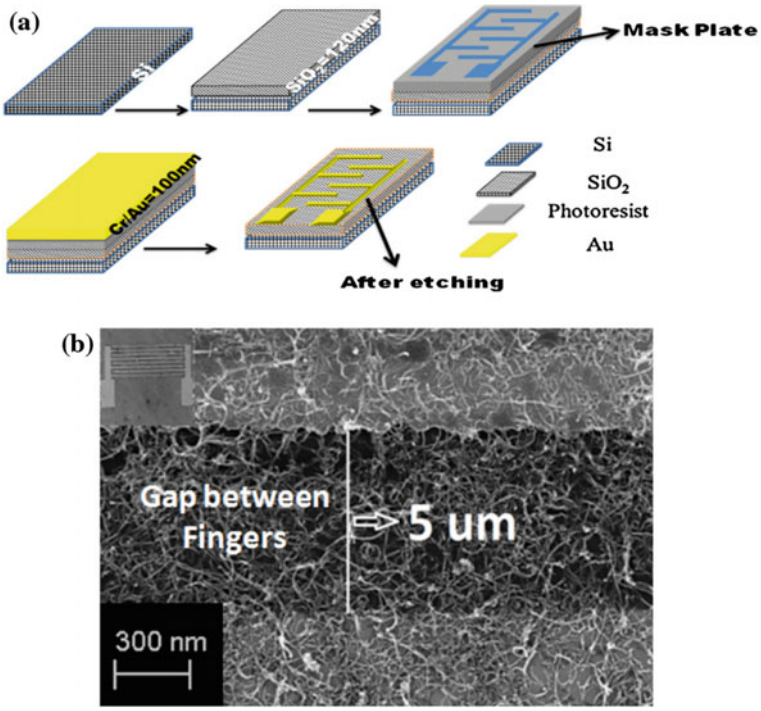

Fig. 4.15 **a** Schematic diagram of fabricated device and **b** SEM image of fabricated interdigitated electrodes [23]

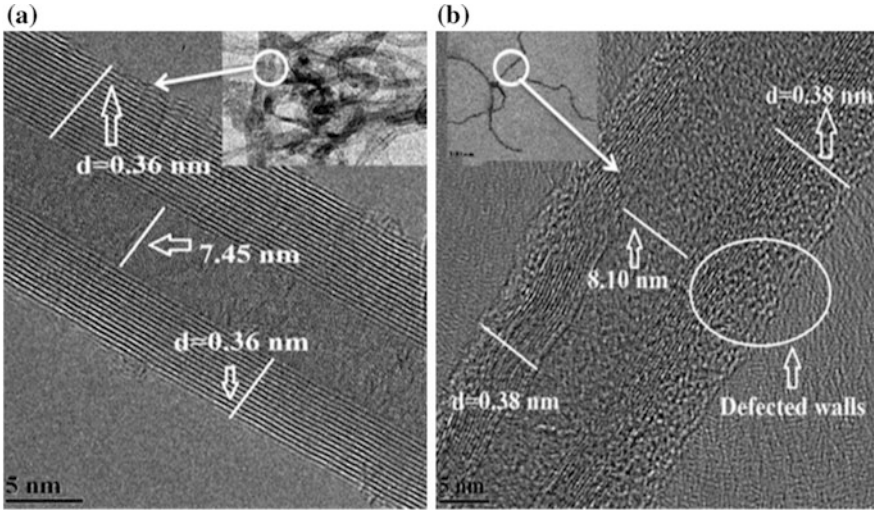

Fig. 4.16 HR-TEM images of **a** P-MWCNTs and **b** F-MWCNTs [23]

control over the number of printing drops and the dropping position. Since SWCNTs adhere to various bare surfaces without any bias due to van der Waals interactions, SWCNT arrays on SOI-wafer were not removed even after liftoff technique providing reliable assembly. Electrode patterning after inkjet printing results in uniform deposition and low contact resistance. The sensor was tested for NO_2 achieving 3% sensitivities with fast recoveries.

Applications of CNT gas sensors depending on conductance change induced by charge transfer from gas molecules absorbed on their surface are limited due to difficulty in detecting gases with low adsorption or low electronegativity. Gas sensors using CNTs have been reported, which work by fingerprinting the ionization characteristic of each individual gas regardless of adsorption energy and electronegativity [25]. The sharp tips of CNTs generate very high electric fields at relatively low voltage, about several hundred volts, which is several-fold lower than the one required with traditional electrodes. Baghgar et al. reported a new type of CNT gas sensor that works in low voltages and low pressures based on bent CNTs grown by rotating the sample relative to applied electric field during growth time. Si samples with (100) orientation for growing CNTs were first cleaned; then, a thin layer of nickel as catalyst was deposited by e-beam evaporation at a base pressure of 3×10^{-6} Torr and temperature of 250 °C. A heat treatment at 730 °C in the presence of H_2 at a pressure of 7 Torr for about 15 min was done in a PECVD system followed by application of hydrogen plasma to form nickel nanoislands. C_2H_2 was introduced as the carbon source for CNT growth at a flow rate of 50 sccm. By rotating the sample, the angle between the direction of applied electric field and the sample changes resulting in the change of growth direction of nanotubes producing bent CNTs with controllable bending angle. A few modifications to the above-discussed process allow the use of as-fabricated device as a gas sensor. A 100-nm-thick SiO_2 layer is thermally grown over Si substrate followed by deposition of a nickel layer. This allows electrical insulation of CNTs from the

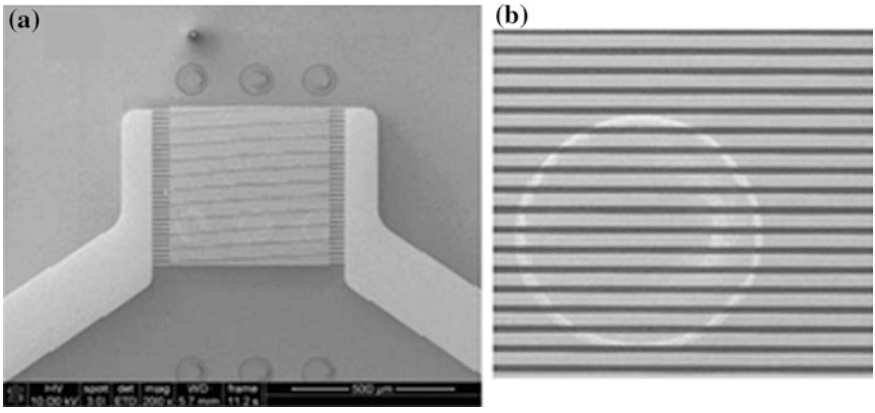

Fig. 4.17 SEM image of inkjet-printed SWCNT gas sensor **a** patterned CNT films under the Pt electrode and **b** dried CNT dropping between electrode fingers [24]

substrate. Then, a 100-nm-thick gold electrode was deposited on the nickel layer using an RF sputtering system. Gold layer was patterned by standard photolithography, over which bent CNTs were grown by the above-discussed process. It was found that by monitoring the current–voltage curve, gas can be identified with far better sensitivity than vertical CNTs due to anode–cathode spacing of less than 100 nm.

Huang et al. [26] reported use of CNTs as gas ionization sensors for ammonia detection based on fingerprinting ionization characteristics of different gases. Strong electric fields generated at the tips of positively and negatively biased CNTs were used to field-ionize or electron impact-ionize ammonia followed by measurement of prebreakdown current. Target gases were detected by monitoring the prebreakdown current. Gas ionization sensor was made of CNT film or zinc oxide (ZnO) rod as one of the electrode and an indium tin oxide (ITO) as the other electrode, both being separated by a glass insulator. The CNT film was grown on silicon substrate by CVD of diameter 30–40 nm. The sensor was placed in a shielded chamber through which air could be pumped out and ammonia could be injected in. It was found that the sensor was selective to ammonia and also showed a linear relationship between prebreakdown current and ammonia concentration with short response and recovery times. CNT films were found to be relatively stable during the measurement process.

4.3.2 Biosensors

Janagama et al. [27] demonstrated a method for fabrication of sensitive protein biosensor using MWCNTs. The developed sensors were used for early detection of prostate-specific antigen (PSA) and breast cancer. CNTs surface modified by carboxylic group was non-covalently attached to surface of clean glassy carbon electrode (GCE). Carboxylation of MWCNTs was done by mixing the carbon nanotube with concentrated nitric acid followed by reflux heating for a few hours. Acid was removed by cleaning in deionized H_2O, and later, nanotube was dried in a stream of nitrogen gas. Glassy carbon was coated on silicon wafers by a photoresist carbonization technique. Biofunctionalization of the above-mentioned structure was carried out by adding anti-S-100 antibodies. The amide group of protein molecule reacts with –COOH groups on MWCNT forming $CONH_2$ having a double bond between carbon and oxygen. The captured protein molecules were hybridized and detected by microscopy.

Higher skin penetration depth of near-infrared (NIR) region makes this frequency range useful for biomedical applications. CNTs are highly attractive for infrared sensors due to their unique structural properties. Semiconducting CNTs can be used as IR detectors as they have bandgap in the IR range. Already developed sensor based on single CNT had relatively low current response because of small sensing area. Enhancing the electric field could be of help, but doing so in the nanoscale is challenging. Fung et al. [28] reported a nanoantenna to increase response of the

sensor with a tenfold increase in photocurrent. Nanoantenna consisted of two symmetric thin metal wires separated by a nanometric gap. Illumination by an infrared source generated a standing wave current pattern along the metal wires. Field in the vicinity of electrically conducting object was enhanced and the CNT sensing element was aligned to the position of maximum estimated field near the antenna, i.e., the point perpendicular to antenna axis. For fabrication, a pair of Au microelectrodes was evaporated on quartz substrate by thermal evaporation and titanium was used to improve the adhesion of gold to the substrate. A drop of CNT suspension was dispersed on the substrate, and CNTs were formed between the electrodes by dielectrophoretic force on application of AC voltage. CNT-metal contact has to be aligned with the maximum field position of antenna. Position of CNT-metal electrode was estimated by AFM. A parylene C thin-film layer was conformally coated at room temperature on CNT for separating the antenna and sensor, also covering CNTs from contamination. The titanium layer for antenna was then patterned and aligned to the sensing region by e-beam lithography. Finally, a pair of thin metal wires was deposited over parylene C layer by thermal evaporation followed by liftoff process to form the nanoantenna. Schematic structure of a CNT-based IR detector with a nanoscale antenna is shown in Fig. 4.18a and AFM images of the fabricated CNT-based IR detector are shown in Fig. 4.18b.

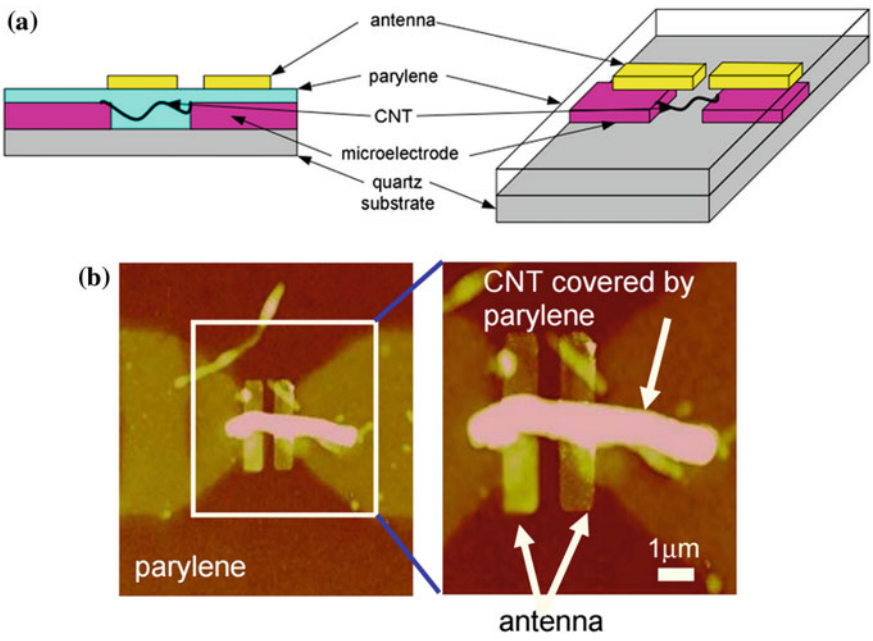

Fig. 4.18 **a** Schematic structure of a CNT-based IR detector with a nanoscale antenna and **b** AFM images of the fabricated CNT-based IR detector with the nanoantenna where parylene thin film was coated between the antenna and CNT [28]

4.3.3 Optical Sensors

Sharma et al. [29] reported near-infrared (NIR) sensors based on SWCNTs on flexible substrates. Sodium dodecyl-benzene sulfonate (SDBS) aqueous solution (formed by mixing SDBS with deionized water) was mixed with SWCNT. The solution was then sonicated for 45 min with a spherical tip at 25 °C for dispersing SWCNT in the aqueous phase. This was followed by centrifugation where heavier particles were found to settle down and then extracted for thin-film deposition on flexible polymer substrate to form the NIR sensor. Substrate was cleaned by ethanol and DI water and dried in N_2. It was covered with an isolation foil with a small window and the sonicated SWCNT was drop casted. The films were dried overnight, and the isolation foil was carefully removed. It was observed that the absorption peaks occurred at the same wavelength for all samples independent of wt % of SWCNT resulting in a uniform dispersion. Optical properties of the dispersions and films were considered. A linear response with a bias up to 5 V was shown for photocurrent. When intensity of the laser increased, more photons were absorbed and more excitons (bound electron-hole pairs) were generated resulting in large current. It was observed that low SWCNT wt% films were more sensitive to NIR illumination than the high wt% SWCNTs. The sensitivity increases with increasing NIR illumination intensity as more photons were absorbed causing large change in photocurrent. The device can be considered reliable as the film showed stable and reproducible response during long-time measurement.

4.3.4 Microelectronics

Earlier developed CNT field-effect transistors (CNFET) were mostly of p-type or ambipolar which was either due to hole doping by environmental oxygen or lower Schottky barrier for hole current at metal-CNT contact. However, to achieve operations of CMOS, well-defined n-type transistors were also needed which requires more reliable and practical methods of fabrication than those already available. Oh et al. reported that the deposition of Al layer on top of a CNT by sputtering under high vacuum gave *n*-type transport properties in CNFET [30]. A schematic of the device structure is shown in Fig. 4.19. High-purity double-walled CNT (DWCNT) and SWCNT were synthesized by hydrogen arc discharge method with diameters in the range of 2 to 4 nm and 1 to 2 nm, respectively. A droplet of dichloroethane containing CNTs was spun over Si substrate with 300-nm-thick thermally grown SiO_2 layer. 30 nm of Pd was deposited by magnetron sputtering at a base pressure of 10^{-8} Torr to form source and drain regions, followed by a standard liftoff process. Then, 30-nm-thick Al was deposited by the same method as Pd. The electrical transport properties of the device at room temperature in vacuum condition showed n-type behavior. It was found that the device formed with Al layer deposited by e-beam deposition at base pressure of

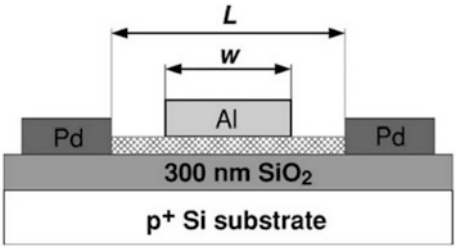

Fig. 4.19 Schematic of the device structure [30]

10^{-6} Torr did not show transfer from *p*-type behavior to *n*-type due to oxidation of Al layer during or after film deposition. This may cause holes to be induced rather than electrons, as oxidized Al surface has work function closer to that of Au. *P*-type behavior of samples is largely due to the large work function of the Pd electrodes causing the Fermi level to be located close to the valence band edge. Ambipolar behavior is due to smaller bandgap edge of large diameter CNT. However, *n*-type doping was obtained due to electron doping caused by the deposited Al layers, as electron charge transfer occurs from Al layer to CNT when unoxidized Al particles are in the vicinity of CNT. This results in the Fermi level being close to valence band edge near Pd electrode and conduction band edge under deposited Al layers causing sharp band bending near the edges of Al layers.

Field-effect transistors (FETs) using SWNTs as a channel are compatible with flexible plastic substrates in the form of thin-film transistors (TFTs) with random networks or aligned arrays of SWNTs. The SWNT films can be formed onto plastic substrates by low-temperature processes such as solution casting and transfer printing. Nouchi et al. [31] fabricated *n*- and *p*-type SWNT TFTs employing solution processes and succeeded in constructing CMOS logic circuits. In this study, *n*- and *p*-type TFTs were fabricated on different substrates by PEI (polyethyleneimine) and (tetracyano-*p*-quinodimethane) TCNQ doping, respectively. By employing an inkjet printing method, it was possible to integrate SWNT TFTs of both polarities onto the same substrate by local deposition of donor or acceptor molecules.

Transparent conductive films (TCF) find a wide range of applications as electrodes for resistive touch screen, projected capacitive touch screen, electronic paper display, as materials for organic light-emitting diode (OLED) displays, OLED lighting, and photovoltaics. CNTs are one of the alternatives for ITO, one of the widely used TCF materials, as indium is a rare metal and ITO being a brittle inorganic material oxide may result in bending, crack formation, and very low electric conductivity of ITO-based TCFs [32]. Compared to SWCNTs and MWCNTs, DWCNTs have the advantage of being transparent electrode material as they can be easily purified by simple chemical treatment. DWCNTs with purity >90% and diameter in range of 1.5 to 2 nm, synthesized by catalytic high-temperature CVD, were chosen as the starting material. Carboxyl methyl cellulose sodium salt (CMC) was chosen as the dispersant. DWCNT was dispersed in it using a tip-type sonicator and ultracentrifugated, and the sediment was

redispersed in water. The DWCNT dispersion was then diluted in water, and the solution was cast on a polyethylene terephthalate (PET) film and heated at 125 °C for 1 min. It was observed that by controlling factors such as CNT length, dispersion states, and weight-rations of the dispersant CMC/DWCNT, TCFs of low surface resistivity (320 Ω sq^{-1}) and 94% transmittance could be obtained without the use of any chemical doping for reducing surface resistivity.

For applications of nanotubes in microelectronics, the most interesting features are the ballistic transport of electrons and the extremely high thermal conductivity along the tube axis. However, high growth temperature (>600 °C) is incompatible with microelectronics along with poor adhesion between CNT and substrate. The open-ended multiwalled CNT arrays could carry higher current density than close-ended CNTs, since the internal walls can participate in the electrical transport. Multichannel ballistic transport could be achieved if the caps of the CNTs are removed (opened), improving CNT electrical conductance. Zhu et al. [33] reported a process for opening CNTs by water-assisted selective etching. They successfully applied the transfer technology to assemble the fine-pitch CNT bundles on the copper substrate with diameter, aspect ratio, and pitch of 25 μm, 4, and 80 μm, respectively. Due to the low process temperature, CNT transfer technology shows promising applications for positioning of CNTs on temperature-sensitive substrates, and for the fabrication of field emitters, electrical interconnects, thermal management structures in microelectronics packaging. Another method for improving adhesion between CNT and substrate was specified by Huang et al. [34] wherein they applied self-assembled monolayer of 3-aminopropyltriethoxysilane (APTS) to modify TSMC CMOS chip surfaces and increase adhesion. The chemical adhesion of CNTs to the surface treated was due to the presence of positive charges or amine groups on the surface. Zhu et al. claimed that the sensor device output measured with different voltage supply by using picoammeter revealed a CNT-based sensor device that could be integrated into CMOS IC at low temperature.

CNTs can function as active material in nanoelectronics and nanoelectromechanical systems for which integration of CNT with microsystems is required. CNT-microsystem integration is hindered by high process temperature required for the same, as processed MEMS/CMOS devices cannot be exposed to temperatures above ~300 °C in post-processing. Existing methods of integration are not feasible as an industrial process due to factors like cost, batch production. Aasmundtveit et al. [35] proposed a method based on CVD and localized heating. A microstructure of two suspended polysilicon microbridges, 5 μm wide and 160 μm long, separated by 15 μm and suspended 3.5 μm above the substrate, was chosen. Fe and Ni were deposited to serve as catalysts. A local electric field was established between the two bridges to guide the direction of growth along with resistive heating on the growth structures. Acetylene (C_2H_2) was chosen as the carbon source as it allowed CNT CVD growth at somewhat lower temperatures than other carbon-containing gases. Temperature at the center of the microbridge was monitored by measuring the resistance, as doped Si showed temperature-sensitive resistivity. Direct Si-CNT integration depicted a potential method for a nanomaterial-based NH_3 sensor.

4.3.5 Supercapacitors

Energy storage capacity of supercapacitors can be increased by using electrodes with large specific surface area and CNT has suitable properties for such applications. CNT forests can have a vertically aligned conformation, and thus, transfer of ions between individual CNTs occurs with ease. Various methods for fabrication have already been reported, and the study by Jiang et al. [36] was advantageous in various aspects compared to previous works. The fabrication started with e-beam evaporation of molybdenum (Mo) over thermally oxidized silicon substrate followed by e-beam evaporation of catalyst (Al and Fe). Then, the substrate was placed in a vacuum quartz tube, purged with hydrogen and raised temperature to 720 °C under atmospheric pressure. Once the temperature was stabilized, hydrogen and ethylene were flown through the quartz tube and CVD was occurred at constant temperature and pressure. As a result, a vertically self-aligned CNT forest was grown and contacted by Mo, the metal current collecting layer. Preferred bending direction was obtained by mechanically pressing the CNT forest. Then, it was submerged in DI water until the CNT-Mo layer was detached from the substrate as adhesion between Mo and oxide layer was weak. The CNT-Mo structure was picked up by a flexible substrate in an aqueous environment and then dried completing the fabrication process. It was observed that there was no change in the height and morphology of CNT forests after 40 electrochemical cycling tests. Since the product supposed to function as a mechanically flexible energy storage device, change in resistance with bending was tested and was found to be essentially stable. The prototype supercapacitor was measured to have a specific capacitance of 7 mF/cm^2. The released CNT-Mo layer patterned into comb drive fingers floatingly loosely above the growth substrate is shown in Fig. 4.20.

4.3.6 Mechanical Properties of Measurements

Hu et al. [37] presented a simple molding process to realize a capacitive-type flexible sensor using 3D CNT interdigitated electrodes. These sensors can be used

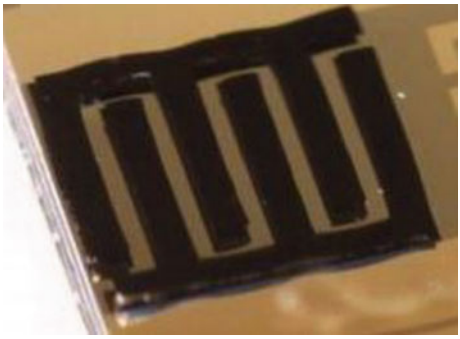

Fig. 4.20 Released CNT-Mo layer patterned into comb drive fingers [36]

for the detection of strain, bending curvature, tactile force, and proximity distance. Silicon substrate was the starting material, over which oxide was deposited and patterned for defining deep reactive ion etching (DRIE) regions. Then, Cr film was evaporated and patterned as the etching mask that defined the support structures for tactile/proximity sensors followed by patterning of photoresist that defined the shape and gap of finger electrodes, resistors, electrical routings, and supports. DRIE process patterned the trenches of the supports on the silicon substrate. Wet etching of Cr opened the finger electrode region. This substrate was the mold for the processes to follow. Fe film of 10 nm thick was deposited and patterned by a photoresist liftoff process, which acted as catalyst for CNT growth. Acetylene pyrolysis in a gas mixture of NH_3 and C_2H_2 at 800 °C made the CNT growth to a height of about 70 μm in regions with catalyst Fe film, filling the trenches and obtaining a highly structured 3D surface topography. SEM micrographs of top and cross-sectional views of the Si substrate patterned by DRIE with patterned Fe catalyst are shown in Fig. 4.21a, b, respectively. A polymer molding process was done to form CNT-polymer composite structures. Amorphous carbon, the by-product of pyrolysis process, was removed by O_2 plasma as it would increase adhesion between polymer, poly-dimethylsiloxane (PDMS), and Si and cause difficulty in their de-molding. In the polymer molding process, PDMS was poured onto Si mold with 3D CNTs, and air trapped inside the trenches was fully removed by a vacuum pump. The attached molds were cured at 100 °C for 1 h, de-molded and the composite structures were manually peeled off by tweezers and released from the Si substrate.

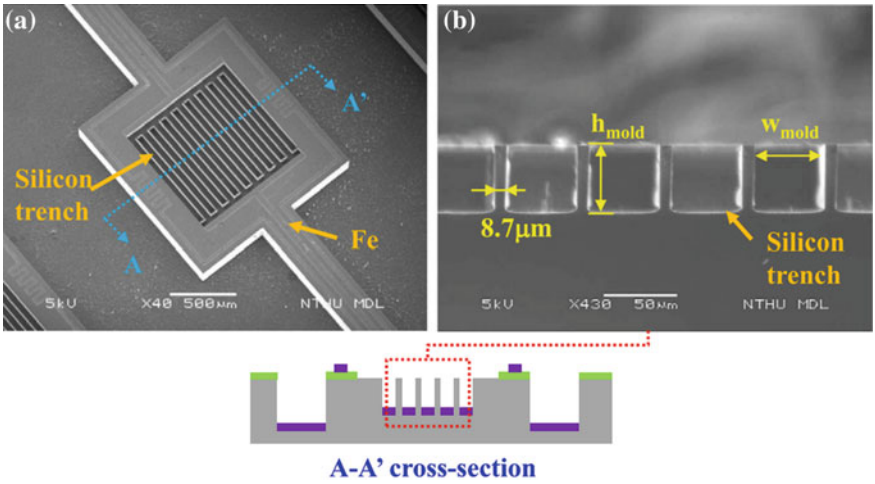

Fig. 4.21 SEM micrographs of **a** top and **b** cross-sectional views of the Si substrate patterned by DRIE with patterned Fe catalyst [37]

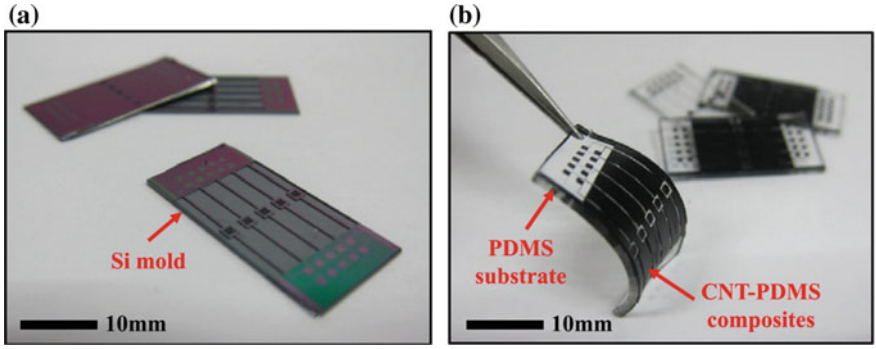

Fig. 4.22 Optical images of **a** the fabricated Si mold and **b** the flexible sensor [37]

The patterned CNTs were transferred to flexible PDMS substrate. Optical images of the fabricated Si mold and the flexible sensor are shown in Fig. 4.22a, b, respectively.

It is known that a mechanical deformation on freestanding SWCNTs leads to strong change in conductance. An AFM tip was used to deform a SWCNT, and it was found that conductance decreased by two orders of magnitude caused by change of bonding configuration from sp^2 to sp^3. The very high elasticity covalent C–C bonds return to its original state even after strong deformation. Stampfer et al. [38] reported a simple configuration of a contacted suspended SWCNT placed under a freestanding cantilever. Deformations of the cantilever due to out-of-plane forces caused the underlying CNT to deform and show change in conductance. Raw SWCNTs were dispersed in aqueous solution of sodium dodecyl sulfate (SDS) surfactant, treated in sonicator, and centrifuged. The upper 75–80% of supernatant was decanted leaving micelle-suspended SWCNT solutions. Si substrate with 1.5 μm oxide layer was spin coated with thin resist layers to enhance liftoff process and was baked at 180 °C. The surface was developed and followed by deposition of 5 nm Cr and 30 nm Au. After lifting off, The surface was functionalized with DAS, *N*-[3-(trimethoxysilyl)propyl]-ethylene-diamine (97%), prior to deposition of CNT, as the Coulomb attraction between positively charged surface due to NH_3^+ and negatively charged CNT resulting from SDS suspension (SO_3^-) enhances deposition. Spin coating followed by e-beam lithography in two steps was used to structure individual devices. First, big core structures that act as anchors in the final device were exposed followed by very fine structures. After development, 0.6 nm Ti and 30 nm (or 50 nm Au) were evaporated followed by liftoff, where Ti layer helps to reduce contact resistance of electrodes. The structure was released by HF etch followed by critical point drying to avoid sticking of freestanding caused by surface tension.

4.3.7 Carbon Electrodes

Electrochemical capacitors (ECs) or "supercapacitors" have many potential advantages in electrical devices by virtue of their large capacitance, high power, and long cycle life. CNTs are suitable materials for polarizable electrodes due to their properties. Ma et al. reported processing of CNT solid electrodes and effect of chemical treatment on the performance of these electrodes in ECs [39]. CNTs were prepared catalytically using Ni catalyst, and nanotubes of diameter 20–30 nm and length up to several tens of microns were obtained. A mixture of CNTs and phenolic resin was molded under a certain pressure. Using the new polarizable electrodes, ECs with specific capacitance of about 15–25 F cm^{-3}, low apparent leakage currents, and low DC resistance were obtained with a single-cell device when the discharge current is about 10 mA. Chemical treatment of the carbon nanotubes and the electrode enhanced the performance of the capacitors. This improvement was related to the surface condition of the carbon nanotubes. It was practical to fabricate ultrahigh capacitors by using such technique. SEM image of fabricated CNT electrode is shown in Fig. 4.23.

Sasaki et al. [40] proposed a direct, planar biological superfunctional nanoelectronic device using CNT electrodes and a standard semiconductor fabrication technique. It performed direct measurement of the electron transport between DNA molecules using as-fabricated CNT electrodes. MWCNTs prepared by arc discharge method and dispersed in solvent were used for the process. The solution containing CNT was coated on Si/SiO_2 wafer by spin-rotational method. Electrical contacts were made with Ti/Au by liftoff process. Focused ion-beam bombardment (FIBB) was used to create a very short channel between the sharply cut edges of the electrode CNT resulting in two closely spaces nanoelectrodes. DNA molecules were then placed between CNT electrodes by electrostatic trapping followed by drying the samples in vacuum and electrical measurement. The current–voltage (*I*–*V*) characteristics showed a very short hopping distance of 3.8 Å, which is similar

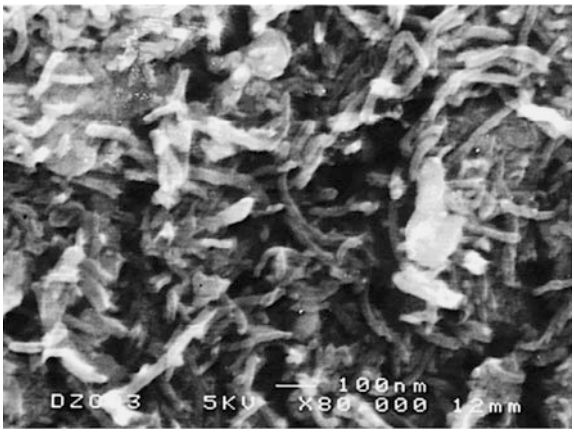

Fig. 4.23 SEM image of CNT electrode [39]

to the distance between general base pairs (~3.4 Å) of poly(*d*G)-poly(*d*C) DNA molecules. The hopping distance measured using metallic electrodes was much longer than the obtained result. Sasaki et al. concluded that the intrinsic direct transport measurement of DNA molecules had been successfully achieved by using CNT electrodes rather than metallic one.

Inanba et al. [41] reported fabrication of nanoprobe electrode-based CNTs for intracellular recording. CNTs are chosen as a potential material for cell studies because of its following properties: mechanical and electrical properties, higher spatial resolution owing to nanoscale diameter, reduction in cell damage due to tube structure, and higher current density. Intracellular recording requires nanoelectrodes insulated over the surfaces other than tips. When parylene-insulated CNT bridges were stretched, inner CNTs slipped while parylene strained. The reason was that the CNTs were grown from both sides forming a bundle structure and that friction coefficient between CNTs was low. Thus, the bridges were cut into probes and CNTs were exposed at the tips by physical stretch. Parylene was suitable as insulator of the CNT electrode, because it was deposited conformally on 3D nanostructure and also it was chemically stable and biocompatible. SEM images of before and after cutting of bare CNT bridges and a parylene-coated CNT bridge are shown in Fig. 4.24a, b, respectively.

Detection of dopamine (DA) is necessary for various biomedical needs and existing methods of detection suffers several drawbacks. The electrode surface could be modified with transition metal complexes and CNTs to enhance the electrochemical performance such as dopamine detection. Yang et al. [42] modified the electrode with $[Co(phen)_3]^{2+}$ and MWCNTs and showed good electrocatalytic activities toward oxidation of DA and possibility of DA detection. For fabrication, glassy carbon electrode (GCE) was polished to mirror-like surface, cleaned ultrasonically, and dipped in acid solution to remove residues. Suspension of MWCNTs was dropped over the electrode to modify it. Electropolymerization of Co

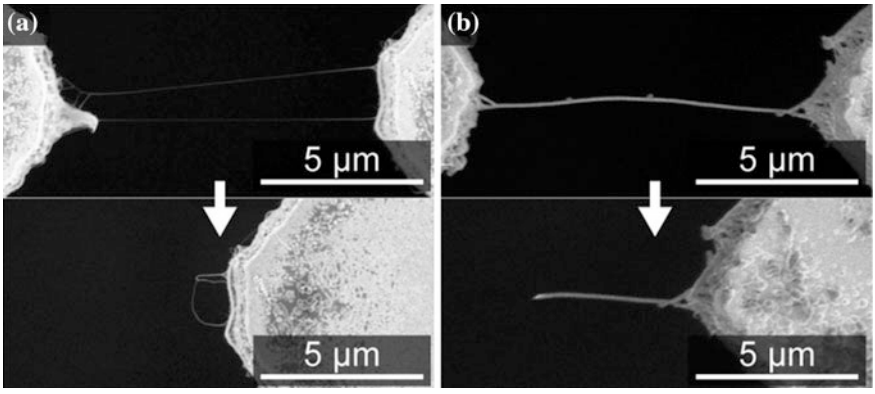

Fig. 4.24 SEM photographs of **a** before and after cutting of bare CNT bridges and **b** a parylene-coated CNT bridge [41]

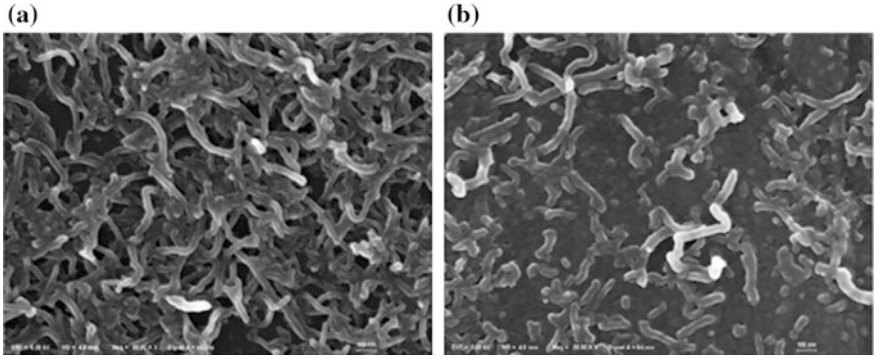

Fig. 4.25 SEM image of **a** MWCNTs/GCE and **b** $[Co(phen)3^{2+}$/WCNTs/GCE [42]

(II) complex was done on the surface by cyclic potential scanning to obtain the electrode $[Co(phen)_3]^{2+}$/MWCNTs/GCE. This modified electrode increased the oxidation peak current with a rapid current response, high sensitivity, good selectivity, and linear response current. SEM images of MWCNTs/GCE and $[Co(phen)_3]^{2+}$/MWCNTs/GCE are shown in Fig. 4.25.

4.4 Carbon-MEMS/NEMS

Carbon-MEMS/NEMS research is new compared to CNT research. It started 20 years ago and has received enormous attention because carbon-MEMS/NEMS provide solutions to some of the major problems presented by CNTs: the difficulty in making ohmic contact, selecting for a precise tube diameter, selecting for a precise tube length, and positioning accuracy. CNTs are typically fabricated on a flat substrate, and the interference of the substrate with the CNT proper functioning is unavoidable. Post-processing metallization on precisely positioned wires is a necessary step to make ohmic contacts to CNTs and variability of contact resistance from CNT sample to sample also remains a major problem. With C-MEMS, it is easy to fabricate CNWs suspended between carbon electrodes, solving the surface interference problem, and making for better sensor and electronic component performance. Additionally, ohmic contacts are automatically established during carbon–carbon bond formation in the carbonization process. We will discuss about some special CNW processes which enable the fine-tuning of wire thickness, length, and position. In contrast, CNTs after synthesis often come with a distribution in lengths and diameters, so they must be isolated and then carefully nanopositioned for integration. This constitutes a low-throughput technique and is unacceptable for mass manufacturing of solid-state devices [43–46].

Several microfabrication methods are available for the development of nanowire, including template methods, ion and electron beam processes, catalytic growth,

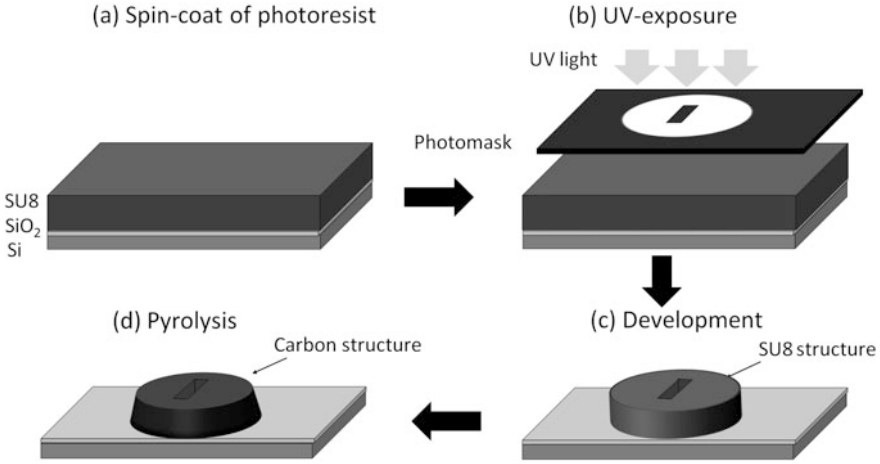

Fig. 4.26 Illustration of C-MEMS: photolithographic patterning of SU-8 photoresist and pyrolysis

Langmuir–Blodgett (LB), chemical liquid deposition (CLD) and CVD, DC arc discharge, and C-MEMS. We will discuss only about the C-MEMS method next.

Shaping of most carbon allotropes into micro- or nanodevices with mechanical machining techniques is not an easy task because the material is usually hard and brittle. Polymers, on the other hand, can be machined easily in a wide variety of machine tools and then converted to carbon devices through pyrolysis, resulting in shapes that are often impossible to make in carbon by any other means. The underlying principle of C-MEMS is to choose an easy to work with polymer precursor, machine, or photopattern this precursor material, and then convert it to carbon using a high-temperature process called pyrolysis.

An example of photolithography process to fabricate C-MEMS structures is illustrated in Fig. 4.26. The process includes spin coating, soft bake, near-ultraviolet (UV) exposure, post-bake, and development. Soft bake and post-bake are not shown in the figure. After the photolithography steps, C-MEMS architectures are obtained in a pyrolysis process. The pyrolysis is carried out in an open-ended quartz-tube furnace, where the samples are baked in an N_2 atmosphere. The pyrolysis process is as follows: first the samples are placed inside the furnace tube and N_2 gas flow is injected with high flow rate at least for initial 15 min to ensure that the environment is inert. Then, the temperature is increased to 300 °C at 5 °C/min ramp rate and is maintained it for 1 h. The temperature is further increased to 900 °C and is maintained for one more hour for carbonization. The whole process of temperature ramping and dwelling must be carried out in the presence of N_2. After that, the furnace is cooled down to 300 °C at a rate of 10 °C/min and the heater is turned off. Finally, the samples are cooled down only by the N_2 flow to reach room temperature.

The resulting microstructure of the carbon material from the process detailed above was found to be glassy carbon (GC). GC has good resistance to high temperatures, low density, low electrical resistance, and relatively high hardness and high resistance to chemical attack, and these properties make GC special for biological, chemical, and many other applications. We will see in the following that CNWs can be made from the same carbon precursor, SU8; this is a very advantageous process characteristic because the integration of CNWs with the supporting structure is rather simple. SU8 is a negative tone photoresist and has the flexibility to fabricate almost any desired design through conventional photolithography and this is followed by pyrolysis as addressed above.

4.4.1 Supporting Structure Fabrication for CNWs

In the late 1990s, Schueller, Brittain, and Whitesides first introduced carbon microstructures fabricated using pyrolysis of a micromolded precursor polymer [47]. In 2002, Singh et al. [48] fabricated C-MEMS structures using negative photoresist, SU8, on silicon wafers for the first time. Since then, various complex high aspect ratio C-MEMS structures such as posts, self-organized bunched posts, and carbon beams supporting wires, and interdigitated electrodes have been developed [46, 49, 50]. The fabrication of the supporting structures (electrodes) for suspended CNWs has already been discussed above.

4.4.2 Electrospinning for Polymer Fibers

Electrospinning is a straightforward and cost-effective method to produce CNWs with diameters ranging from less than 3 nm to more than 1 mm [51], and the electrospinning experiments can be performed by using simple setups. Electrospinning can be applied to the fabrication of NWs made from materials as diverse as synthetic and natural polymers, polymer alloys, polymer composites, as well as metals and ceramics [52]. Some of the current electrospinning applications include filtrations [53], advanced fabrics (e.g., for wound dressing [54]), scaffolds [55, 56], medical implants [57], fabrication of micro- or nanodevices such as field-effect transistors [58, 59], and gas sensors [60, 61].

4.4.2.1 Electrospinning Setup Description

A conventional electrospinning setup is shown in Fig. 4.27. It consists of four key components: a high-voltage power supply (working range between 10 and 30 kV), a polymer precursor reservoir, a conductive dispensing needle, and a conductive substrate. The reservoir maintains a constant polymer solution flow rate through

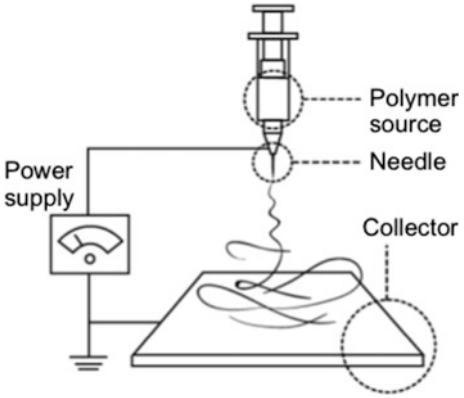

Fig. 4.27 Schematic of traditional electrospinning setup [51]

dispensing needle, a syringe, which is connected to either a mechanical or a pneumatic syringe pump. The conductive dispensing needle acts as the polymer source, which is connected to a high-voltage power supply. The needle is also sometimes called tip, nozzle, or spinneret, and its internal diameter is often in the range of hundreds of micrometers. The conductive substrate is normally grounded and serves as a collector for the electrospun NWs (Fig. 4.27).

When a voltage, higher than 10 kV, is applied to the needle, the polymer solution at the needle tip becomes unstable and a polymer jet is formed. Initially, the jet flows away from the needle in a nearly straight line, and then, it bends into a complex path during which electrical forces stretch and thin it to the nanometer scale. The initial straight section of the jet is known as near-field regime and the area where the electrical instabilities dominate is called the far-field regime. The schematic of the path of the fiber (NW) jet is shown in Fig. 4.28.

The key stages of the polymer jet formation in the electrospinning process are (a) droplet formation, (b) Taylor cone formation, (c) launching of the jet, (d) elongation of straight segment, (e) whipping instability, and (f) solidification into NW [62]. These stages are described in detail in [63].

4.4.2.2 Dimensions of the Nanowires

The morphology and dimensions of the fabricated polymer fibers depend on the composition of the electrospun polymer and the solution concentration. The more diluted solutions generate the thinner fibers and the concentrated solutions produce the thicker fibers. If the polymer concentration is too low, beads are formed instead of fibers, and with the very high concentrations, electrospinning might not be possible. Generally, the dimensions of the polymer fibers depend on the following parameters: (a) polymer precursor material, (b) polymer solution concentration, (c) needle-to-collector distance, (d) flow rate of the precursor, (e) applied voltage, and (f) mechanical stretching. A typical electrode-to-collector distance varies from

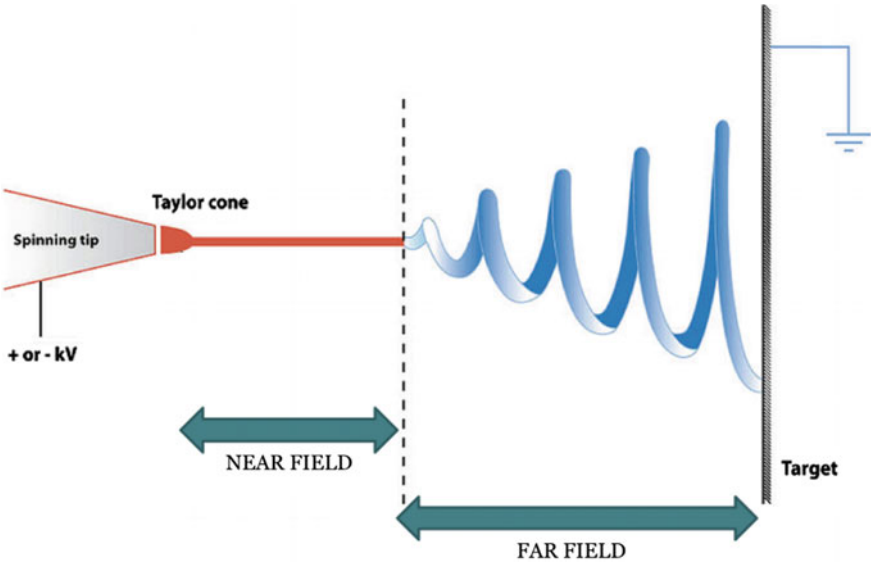

Fig. 4.28 Schematic of the path of the fiber jet. *Courtesy* Wikipedia

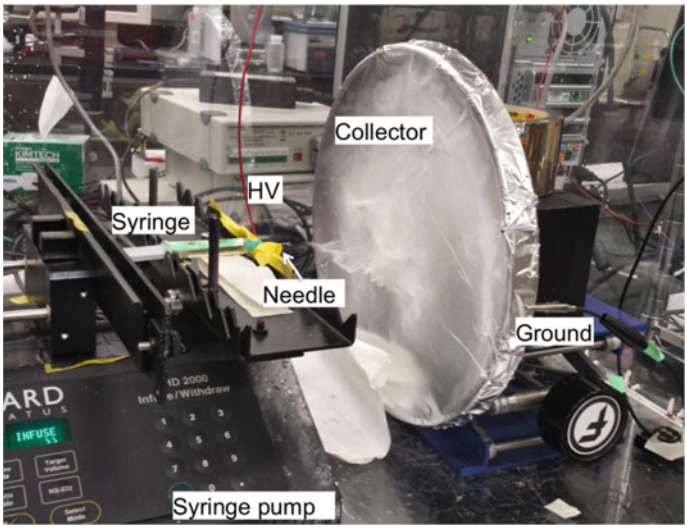

Fig. 4.29 Photographs of UCI BioMEMS Laboratory electrospinning setup [51]

8 to 30 cm. In Fig. 4.29, we show a photograph of the UCI BioMEMS Laboratory far-field electrospinning setup.

In Fig. 4.30, we show a scanning electron microscope (SEM) image of suspended NWs on carbon posts.

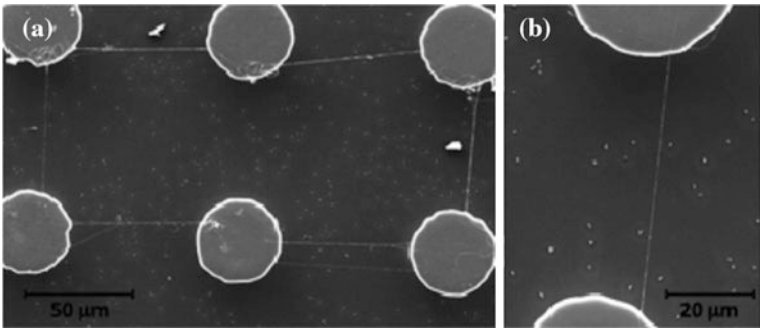

Fig. 4.30 SEM images of suspended nanowires on carbon posts **a** six carbon posts connected each other by nanowires, **b** and individual nanowire [51]

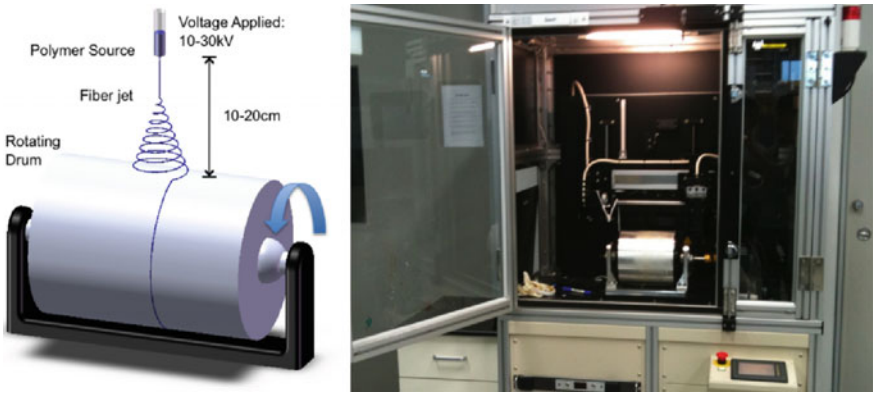

Fig. 4.31 Schematic of an FFES system with rotating drum and commercially available electrospinning setup [51]

In the far-field technique, NWs are randomly deposited on the collector. However, for many applications, highly aligned nanofibers are required. Hence, the alignment of electrospun nanofibers is the most important challenge encountered in the electrospinning field. Kim and Reneker used a rotating drum as collector electrode, aligning the collected fibers in the direction of the drum rotation and producing relatively uniform mats of oriented fibers [64]. In Fig. 4.31, we show a schematic drawing of an electrospinning setup with a rotating drum collector and a picture of a commercially available electrospinning system.

The electric instabilities inherent in FFES make this process inappropriate for a wide range of applications that require isolated NWs to be deposited in a controlled pattern or to be deposited only in predetermined locations. Near-field electrospinning (NFES) technology was developed to fill the demand for production of micro- and nanofibers with increased positioning precision [65–67]. The distance between the fiber source and the collector is significantly reduced for NFES and this

reduction in distance allows for depositing the fibers on the substrate before the onset of the whipping motion. But for NFES, the applied electric field is unable to provide enough force to stretch out the fiber jet diameter to the nanometer scale. Only micrometer-sized fibers are produced using the NFES process. Electromechanical spinning (EMS) developed by Madou et al. [68] improves the NFES by offering thinner fibers with an exceptional nanofiber deposition control. The fundamental principle behind EMS is the use of viscoelastic polymer inks in conjunction with a low-deposition voltage and a mechanical pull on the polymer fibers.

4.4.3 Setup Description of EMS

In EMS, this distance is in the range of 500 μm to 1.5 mm, and thus, EMS operates in the stable liquid jet region. Generally, the syringe in the EMS setup is mounted using a syringe holder and this can be manually or automatically positioned in the *x*–*y*–*z* directions. The target is mounted on an *X*–*Y* microstage that can be programmed to move in any desired pattern at different speeds and accelerations. A power supply, shown in Fig. 4.32, is connected to the needle to provide the high voltage and the substrate is grounded. The polymer solution flows through the needle to form a full-sized droplet at the needle tip. The polymer jet does not self-initiate upon the voltage turned, as mentioned earlier. To initiate the jet in

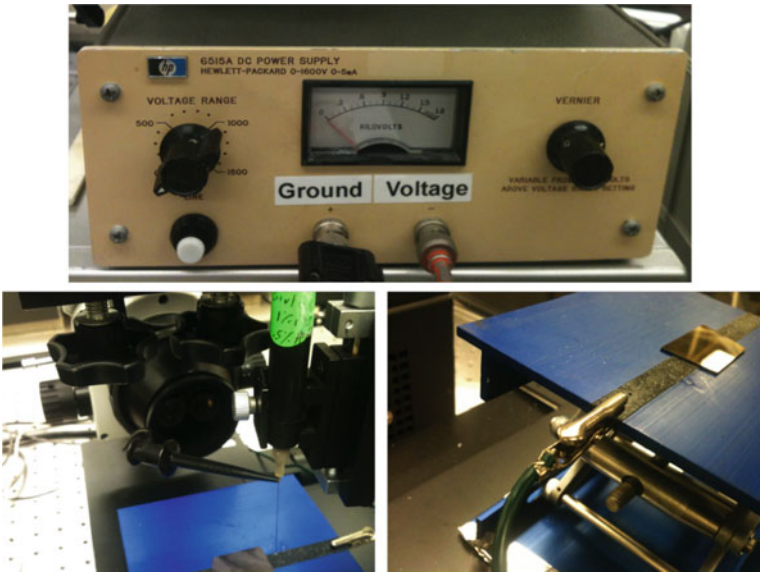

Fig. 4.32 Photographs of voltage supply, syringe, and grounded substrate of EMS setup [51]

EMS, it is necessary to introduce an artificial instability at the droplet–air interface that results in a very high local electric field and if this local electrical field is sufficient to overcome the interfacial surface tension, and then, a jet initiates. This artificial instability can be induced, for example, by poking the droplet with a glass microprobe tip (1–3 μm tip diameter). Once the jet is initiated, the system reaches a new equilibrium with a jet that continues to flow as long as the electric field is applied and new polymer solution is available.

4.4.4 Various Research Works on C-MEMS CNWs

Madou et al. [68] demonstrated far-field electrospinning to fabricate arrays of suspended CNWs by carbonization of polymeric, polyacrylonitrile (PAN) and SU8, nanowires. The nanowires were suspended between specially designed three-dimensional electrodes, posts, fabricated using organic resorcinol-formaldehyde-based xerogel. In Fig. 4.33, we show an SEM image of suspended CNWs.

In Fig. 4.34, we show SEM images of a single suspended nanowire made from SU8 and PAN, suspended between two photographically patterned C-MEMS electrodes. The linear behavior of the *I–V* curves is presented in Fig. 4.34c, showing in both cases an ohmic contact between the electrodes and the suspended nanowires. The conductance was calculated by measuring the slope of the *I–V* curves for both the cases, and it was revealed that PAN-derived CNFs are more graphitic than SU8-derived CNF and, therefore, exhibit higher conductivities.

Madou and a collaborator group in South Korea reported the fabrication of scalable suspended CNW meshes, to use as electrochemical sensing platforms, using the C-MEMS process [69]. A 6-in. silicon wafer with a thermally grown SiO_2 layer was used as the substrate material and the following three photolithography

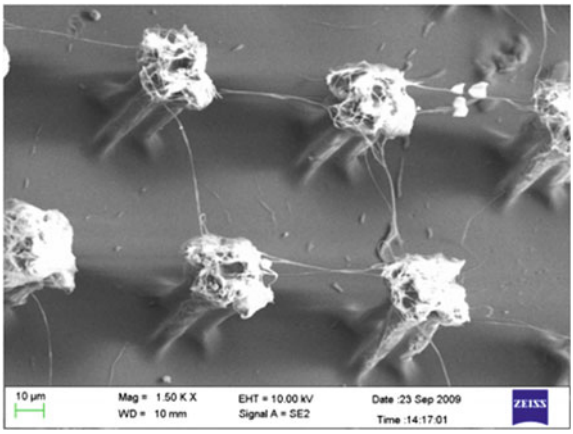

Fig. 4.33 SEM image of suspended CNW on 3D carbon post [68]

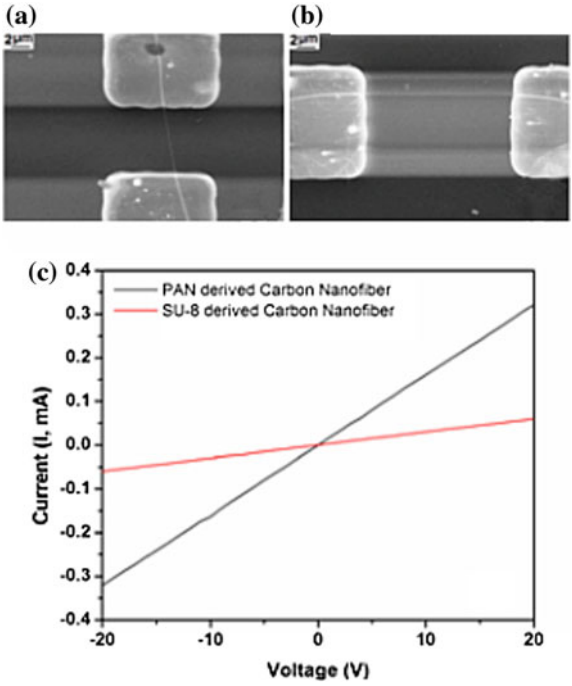

Fig. 4.34 SEM images of single suspended nanowire: **a** Su8 derived and **b** PAN derived. **c** *I–V curve* for the both cases [68]

steps were carried out using SU8 as the resist: (i) define the 4-μm-thick planar polymer pads, (ii) define the tall contact pads to support the suspended photoresist microwire meshes, and (iii) pattern the suspended photoresist microwire meshes bridging the prepatterned photoresist contact pads. Planar electrodes and suspended microwire meshes were released in a single-process step and the completed photoresist structures were converted into carbon by pyrolysis. In Fig. 4.35, we show two SEM images of a group of nanoelectrode set.

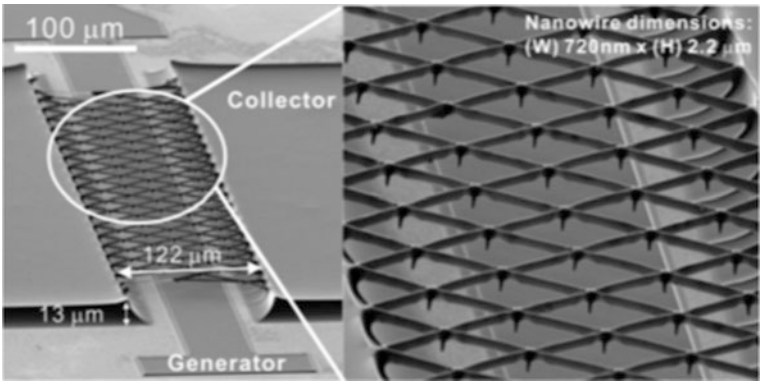

Fig. 4.35 SEM images of nanoelectrode set [69]

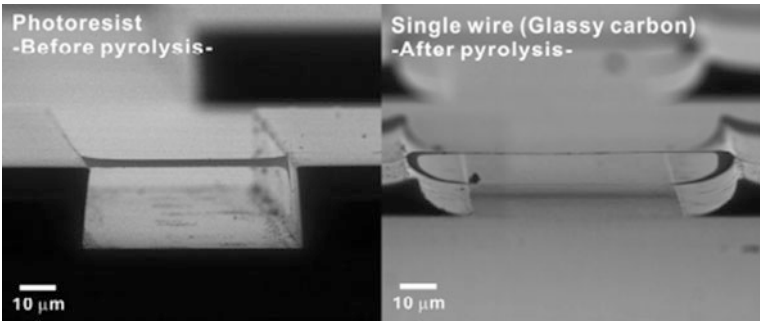

Fig. 4.36 SEM images of photoresist and suspended nanowire structure [70]

Shin et al. reported on the processing of monolithic suspended glassy carbon nanostructures. They also used two common batch processes: UV lithography and polymer pyrolysis [70] to fabricate the carbon structures which include two tall carbon pads and a suspended nanowire bridging the pads. SEM images of single CNWs are shown in Fig. 4.36. A hydrogen sensor based on the above-fabricated nanowire was also reported by the same research group [71]. For the detection of hydrogen, they deposited a thin palladium layer on the suspended CNW.

4.5 Applications of C-MEMS-Based CNWs

Some recent examples of C-MEMS/NEMS applications include electrochemical sensors, substrate for molecular electronics, batteries, fuel cells, dielectrophoretic electrodes, capacitors, scaffolds, nanoconstrictions, molds for bulk metallic glasses, and gas sensors. Here, we provide a short description of the emerging C-MEMS application of suspended carbon hot nanowires to make nanogas sensors with local CVD, nanoconstrictions, and nanogaps.

Suspended CNWs are separated from the supporting substrate, so as free from the substrate influences such as contamination and charge shunting, and this leads to significant advantages over other nanowire-based sensors typically embedded on a solid substrate. The sensing is usually a surface phenomenon and CNWs, having a high surface-to-volume ratio, are approached by analyte molecules from all directions, and this leads to an improved lower LOD. This principle is called wash cloth line sensors. By derivatizing the CNW surface with an appropriate monolayer of sensor molecules, say protein or DNA molecules, the nanowires can be turned nanoimmuno- or nano-DNA sensors. Nanogas sensors can also be made by coating the CNWs surface with metal oxide semiconductors (MOS). A SEM image of a suspended CNW and a schematic of wash cloth line are shown in Fig. 4.37.

Local CVD on the CNW occurs upon applying a direct current to the suspended CNW. The high resistance of the CNW, compared to the bulkier supporting

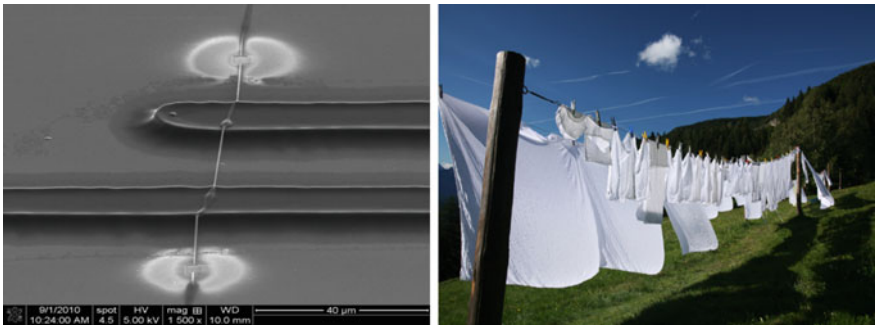

Fig. 4.37 Suspended nanowire (*left*) with a wash cloth line (*right*) [64]

electrodes, allows for its selective heating on the CNW but not on the supporting electrodes. As an example of metal-oxide-semiconductor (MOS) deposition that can be used for the fabrication of a NO_x nanogas sensor, our group has demonstrated the local CVD on CNWs by depositing a tungsten oxide (WO_3) film from tungsten hexacarbonyl [$W(CO)_6$] as the precursor. SEM images of a 358-nm-thick, 30-μm-long CNW after WO_3 deposition by local CVD of $W(CO)_6$ are shown in Fig. 4.38a, b. The thickness of the deposit follows the temperature profile expected for a heated nanowire with the center being considerably thicker (diameter of ~1.8 μm) compared to the ends of the CNW (358 nm).

The local CVD phenomenon illustrated above is not limited to WO_3 deposition. Local CVD on CNWs has the potential to become a useful tool for thermal deposition of many materials selectively on the joule-heated fibers, allowing many types of nanosensors and nanoelectronics devices.

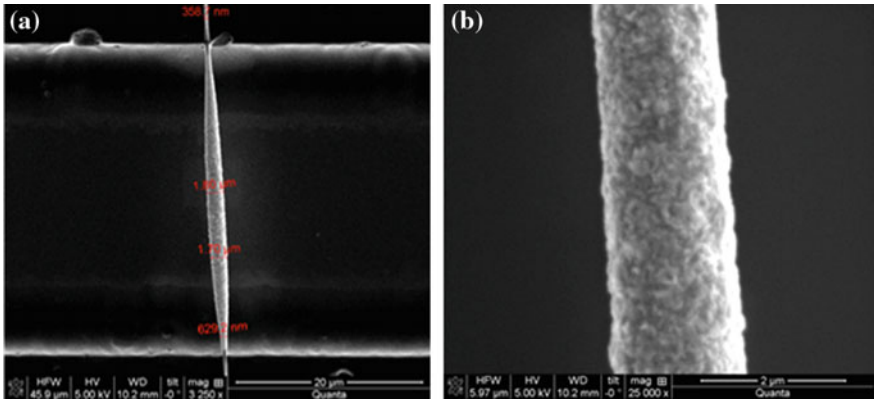

Fig. 4.38 **a** SEM images of a 358-nm-*thick* CNW with WO_3 deposited on its surface by selected area CVD, **b** a high-magnification image of the granular surface of WO_3 [72]

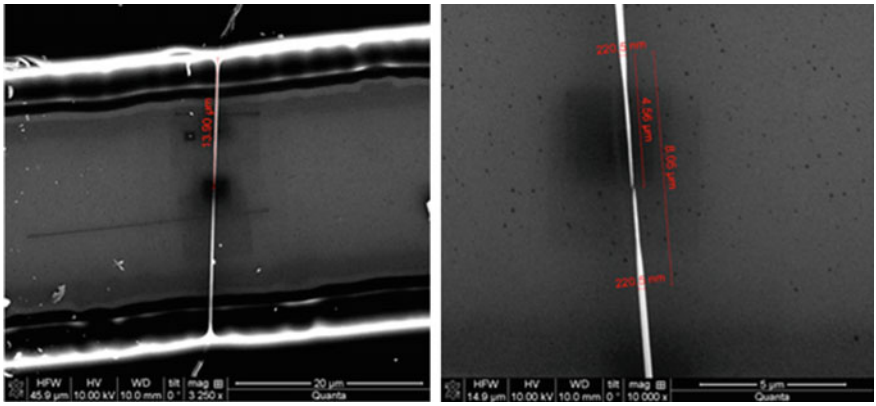

Fig. 4.39 SEM images of a CNW showing breakage due to overheating at its center [72]

Using controlled Joule heating of suspended nanowires, one can manufacture nanogap and quantum mechanical nanoconstrictions without the need for expensive equipment. At the beginning of a Joule heating experiment, a central region of the CNW attains the highest temperature which is high enough to sublimate some carbon from its surface. This thinner segment attains the sublimation temperature even faster with a constant current application, as it offers a yet higher resistance, which will lead to yet faster thinning at its center. Finally, when the center cannot withstand further thinning the nanowire breaks. We show SEM images of suspended CNW which breaks at center upon joule heating in Fig. 4.39.

Our recent study proves that the thinner and shorter CNW has the higher temperature gradient, so as the smaller nanogap in its center. Nanogaps with a dimension of less than 10 nm in a CNW might have great utility as a building block for molecular electronics, based on molecular interactions in a carbon–molecule–carbon (C–M–C) structure. There are a lot of techniques for obtaining nanogaps, but a process to totally control the gap size has not been found yet. We are currently developing an electronic control system to control the wire thickness in the center to any desired radius (nanoconstriction) and to make nanogaps of any size.

References

1. S. Iijima, Helical microtubules of graphitic carbon. Nature **314**, 56–58 (1991)
2. H.H. Kim, H.J. Kim, in *The Preparation of Carbon Nanotubes by DC arc Discharge Process Using Xylene-Ferrocene as a Floating Catalyst Precursor*. NMP47, Nanotechnology Materials and Devices Conference, IEEE, (2006), pp. 496–497
3. Y. Sato, K. Motomiya, B. Jeyadevan, K. Tohji, G. Sato, H. Ishida, T. Hirata, R. Hatakeyama, Effect of cerium ions in an arc peripheral plasma on the growth of radial single-walled carbon nanotubes. J. Appl. Phys. **98**, 094313 (2005)

4. M. Kanai, A. Koshio, H. Shinohara, T. Mieno, A. Kasuya, Y. Ando, X. Zhao, High-yield synthesis of single-walled carbon nanotubes by gravity-free arc discharge. Appl. Phys. Lett. **79**, 2967 (2001)
5. M. Keidar, I. Levchenko, T. Arbel, M. Alexander, A.M. Waas, K.K. Ostrikov, Magnetic-field-enhanced synthesis of single-wall carbon nanotubes in arc discharge. J. Appl. Phys. **103**, 094318 (2008)
6. T. Sugai, H. Omote, S. Bandow, N. Tanaka, H. Shinohara, Production of fullerenes and single-wall carbon nanotubes by high-temperature pulsed arc discharge. J. Chem. Phys. **112**, 6000 (2000)
7. Y. Ando, X. Zhao, K. Hirahara, S. Iijima, Production of thick single-walled carbon nanotubes by arc discharge in hydrogen ambience. AIP Conf. Proc. **590**, 7 (2001)
8. T. Guo, P. Nikolaev, A. Thess, D.T. Colbert, R.E. Smalley, Catalytic growth of single-walled nanotubes by laser vaporization. Chem. Phys. Lett. **243**, 49–54 (1995)
9. A. Thess, R. Lee, P. Nikolaev, H. Dai, P. Petit, J. Robert, C. Xu, Y.H. Lee, S.G. Kim, A.G. Rinzler, D.T. Colbert, G.E. Scuseria, D. Tomanek, J.E. Fischer, R.E. Smalley, Crystalline ropes of metallic carbon nanotubes. Science **273**(5274), 483–487 (1996)
10. J. Chae, X. Ho, J.A. Rogers, K. Jain, Patterning of single walled carbon nanotubes using a low-fluence excimer laser photoablation process. Appl. Phys. Lett. **92**, 173115 (2008)
11. J. Chae, K. Jain, Patterning of carbon nanotubes by material assisted laser ablation process. IEEE Trans. Nanotechnol. **9**(3), 381–385 (2010)
12. T. Wang, J. Shang, J. Liu, in *Preparation of VACNT TIM by a Novel Metallization and Chemical Bonding Process*. 13th International Conference on Electronic Packaging Technology and High Density Packaging (ICEPT-HDP) (2012), pp. 1646–1649
13. B.T. Nguyen, X.T. Than, V.C. Nguyen, T. Thanh, T. Ngo, H.T. Bui, X.N. Nguyen, H.K. Phan, N.M. Phan, Fabrication of horizontally aligned ultra-long single-walled carbon nanotubes on Si substrates using the fast-heating chemical vapour deposition method. Adv. Nat. Sci.: Nanosci. Nanotechnol. **3**, 025010 (2012)
14. Y. Matsuoka, I.T. Clark, M. Yoshimura, Growth mechanism of multilayer-graphene-capped, vertically aligned multiwalled carbon nanotube arrays. J. Vac. Sci. Technol. B **29**(6), 061801 (2011)
15. M.A. Nguyen, D.T. Ngo, V.T. Le, D.V. Cao, Synthesis of single-walled carbon nanotubes over Co–Mo/Al_2O_3 catalyst by the catalytic chemical vapour deposition of methane. Adv. Nat. Sci.: Nanosci. Nanotechnol. **4**, 035018 (2013)
16. S. Ramakrishnan, E.J. Jelmy, A. Baladandapani, M. Rangarajan, N.K. Kothurkar, Synthesis of multiwalled carbon nanotubes using RF-CCVD and a bimetallic catalyst. AIP Conf. Proc. **1447**, 275–276 (2012)
17. J. Lee, S. Choi, in *Fabrication of Carbon Nanotubes by Anodic Aluminum Oxide Nano-template*. NMP12, Nanotechnology Materials and Devices Conference, IEEE (2006), pp. 426–427
18. J. Wu, M. Eastman, T. Gutu, M. Wyse, J. Jiao, S.-M. Kim, M. Mann, Y. Zhang, K.B.K. Teo, Fabrication of carbon nanotube-based nanodevices using a combination technique of focused ion beam and plasma-enhanced chemical vapour deposition. Appl. Phys. Lett. **91**, 173122 (2007)
19. W.K. Wong, C.S. Lee, S.T. Lee, Uniform-diameter, aligned carbon nanotubes from microwave plasma-enhanced chemical-vapour deposition. J. Appl. Phys. **97**, 084307 (2005)
20. G.I. Shim, Y. Kojima, S. Kono, Y. Ohno, T. Ishijima, Fabrication of carbon nanotubes by slot-excited microwave plasma-enhanced chemical vapor deposition. Jpn. J. Appl. Phys. **47**, 5652–5655 (2008)
21. K.S. Kim, G. Cota-Sanchez, C.T. Kingston, M. Imris, B. Simard, G. Soucy, Large-scale production of single-walled carbon nanotubes by induction thermal plasma. J. Phys. D Appl. Phys. **40**, 2375–2387 (2007)
22. J.-T Huang, C.-H Lin, P.-C Chang, in *Low-temperature Fabrication Method of Carbon Nanotubes-Based Gas Sensor*. International Conference on Electronic Materials and Packaging (2008), pp. 57–60

23. S. Dhall, N. Jaggi, R. Nathawat, Functionalized multiwalled carbon nanotubes based hydrogen gas sensor. Sens. Actuators A **201**, 321–327 (2013)
24. J.-H. Yun, H. Chang-Soo, J. Kim, J.-W. Song, D.-H. Shin, Y.-G. Park, in *Fabrication of Carbon Nanotube Sensor Device by Inkjet Printing*. Proceedings of the 3rd IEEE Int. Conf. on Nano/Micro Engineered and Molecular Systems (2008), pp. 506–509
25. M. Baghgar, Y. Abdi, E. Arzi, Fabrication of low-pressure field ionization gas sensor using bent carbon nanotubes. J. Phys. D Appl. Phys. **42**, 135502 (2009)
26. J. Huang, J. Wang, C. Gu, K. Yu, F. Meng, J. Liu, A novel highly sensitive gas ionization sensor for ammonia detection. Sens. Actuators A **150**, 218–223 (2009)
27. D. Janagama, P. Goud, R. Markondeya, M. Iyer, T. Rao, in *Biofunctionalization of Multi-walled Carbon Nanotubes (MWNTs) for the Fabrication of Protein Nano Biosensors*. 11th National symposium on Advanced Packaging Materials: Processes, Properties and Interface (2006), pp. 119–121
28. C.K.M. Fung, N. Xi, B. Shanker, K.W.C. Lai, J. Zhang, H. Chen, Y. Luo, in *Design and Fabrication of Nano Antenna for Carbon Nanotube Infrared Detector*. 8th IEEE Conference on Nanotechnology (2008), pp. 205–208
29. R. Sharma, A. AI-Hamry, S. Vijayragavan, A. Benchirouf, A. Sanli, C. Miiller, O. Kanoun, in *Single-Wall Carbon Nanotubes Based Near-Infrared Sensors on Flexible Substrate*. 11th International Multi-Conference on Systems, Signals and Devices (2014), pp. 1–5
30. H. Oh, J.-J. Kim, W. Song, S. Moon, N. Kim, J. Kim, N. Park, Fabrication of *n*-type carbon nanotube field-effect transistors by Al doping. Appl. Phys. Lett. **88**, 103503 (2006)
31. R. Nouchi, H. Tomita, A. Ogura, H. Kataura, M. Shiraishi, Logic circuits using solution-processed single-walled carbon nanotube transistors. Appl. Phys. Lett. **92**, 253507 (2008)
32. N. Imazu, T. Fujigaya, N. Nakashima, Fabrication of flexible transparent conductive films from long double-walled carbon nanotubes. Sci. Technol. Adv. Mater. **15**, 025005 (2014)
33. L. Zhu, K. Moon, B. Bertram, D.W. Hess, C.P. Wong, in *Assembling Carbon Nanotube Bundles Using Transfer Process for Fine-Pitch Electrical Interconnect Applications*. Electronic Components and Technology Conference (2007)
34. J.-T. Huang, P.-C. Chang, H.-W. Chao, P.-L. Hsu, in *A Low-Temperature Fabrication Process Integrated Carbon Nanotubes-Based Sensor Device into CMOS IC*. IEEE NANO (2009)
35. K.E. Aasmundtveit, B.Q. Ta, L. Lin, E. Halvorsen, N. Hoivik, Direct integration of carbon nanotubes in Si microstructures. J. Micromech. Microeng. **22**, 074006 (2012)
36. Y. Jiang, A. Kozinda, T. Chang, L. Lin, Flexible energy storage devices based on carbon nanotube forests with built-in metal electrodes. Sens. Actuators A **195**, 224–230 (2013)
37. C.-F. Hu, J.-Y. Wang, Y.-C. Liu, M.-H. Tsai, W. Fang, Development of 3D carbon nanotube interdigitated finger electrodes on polymer substrate for flexible capacitive sensor application. Nanotechnology **24**, 444006 (2013)
38. C. Stampfer, A. Jungen, C. Hierold, *Fabrication of discrete carbon nanotube based nano-scaled force sensors* (Sensors, IEEE, 2004), pp. 1056–1059
39. R.Z. Ma, J. Liang, B.Q. Wei, B. Zhang, C.L. Xu, D.H. Wu, Study of electrochemical capacitors utilizing carbon nanotube electrodes. J. Power Sour. **84**, 126–129 (1999)
40. T.K. Sasaki, A. Ikegami, M. Mochizuki, N. Aoki, Y. Ochiai, in *Fabrication of Carbon Nanotube Electrodes for Bio-Nano-Electronic Devices*. IPAP Conference Series 6 (2005), pp. 168–170
41. A. Inaba, Y. Takei, T. Kan, K. Matsumoto, I. Shimoyama, *Nanoprobe Electrodes Cut by Physical Stretch of Parylene-insulated Carbon Nanotube Bridges, Transducers'11* (Beijing, China, 2011)
42. L. Yang, X. Li, Y. Xiong, X. Liu, X. Li, M. Wang, S. Yan, L.A.M. Alshahrani, P. Liu, C. Zhang, The fabrication of a Co (II) complex and multi-walled carbon nanotubes modified glass carbon electrode, and its application for the determination of dopamine. J. Electroanal. Chem. **731**, 14–19 (2014)

43. E.C. Walter, K. Ng, M.P. Zach, R.M. Penner, F. Favier, Electronic devices from electrodeposited metal nanowires. Microelectron. Eng. **61–62**, 555–561 (2002)
44. Y. Chai, Y. Wu, K. Takei, H.Y. Chen, S. Yu, P.C.H. Chan, A. Javey, H.S.P. Wong, *In 2010 IEEE International Electron Devices Meeting (IEDM)* (IEEE, San Francisco, CA, 2010), pp. 214–217
45. J. Huang, Q. Wan, Gas sensors based on semiconducting metal oxide one-dimensional nanostructures. Sensors **9**(12), 9903–9924 (2009)
46. S. Bibekananda, V.J. Babu, V. Subramanian, T.S.J. Natarajan, Preparation and characterization of electrospun fibers of poly(methyl methacrylate)-single walled carbon nanotube nanocomposites. J. Eng. Fibers Fabr. **3**(4), 39–45 (2008)
47. O.J. Schueller, S.T. Brittain, G.M. Whitesides, Fabrication of glassy carbon microstructures by pyrolysis of microfabricated polymeric precursors. Adv. Mater. **9**(6), 477–480 (1997)
48. A. Singh, J. Jayaram, M. Madou, S. Akbar, Pyrolysis of negative photoresists to fabricate carbon structures for microelectromechanical systems and electrochemical applications. J. Electrochem. Soc. **149**(3), E78–E83 (2002)
49. B.Y. Park, R. Zaouk, C. Wang, M.J. Madou, A case for fractal electrodes in electrochemical applications. J. Electrochem. Soc. **154**(2), 1–5 (2007)
50. J.-I. Heo, Y. Lim, M. Madou, H. Shin, in *Scalable Suspended Carbon Nanowire Meshes as Ultrasensitive Electrochemical Sensing Platforms*. IEEE 25th International Conference on Micro Electro Mechanical Systems (MEMS) (2012), pp. 878–881
51. G. Canton, in *Development of Electro-Mechanical Spinning for Controlled Deposition of Carbon Nanofibers*. PhD Thesis, UCI (2014)
52. A. Greiner, J.H. Wendor, Electrospinning: a fascinating method for the preparation of ultrathin fibers. Angew. Chem. Int. Ed. **46**(30), 5670–5703 (2007)
53. P. Gibson, H. Schreuder-Gibson, D. Rivin, Electrospun fiber mats: transport properties. AIChE J. **45**(1), 190–195 (1999)
54. H.-J. Jin, S.V. Fridrikh, G.C. Rutledge, D.L. Kaplan, Electrospinning bombyx mori silk with poly(ethylene oxide). Biomacromolecules **3**(6), 1233–1239 (2002)
55. Q.P. Pham, U. Sharma, A.G. Mikos, Electrospinning of polymeric nanofibers for tissue engineering applications: a review. Tissue Eng. **12**(5), 1197–1211 (2006)
56. R. Murugan, S. Ramakrishna, Nano-featured scaffolds for tissue engineering: a review of spinning methodologies. Tissue Eng. **12**(3), 435–447 (2006)
57. S. Agarwal, J.H. Wendor, A. Greiner, Use of electrospinning technique for biomedical applications. Polymer **49**(26), 5603–5621 (2008)
58. A. Babel, D. Li, Y. Xia, S.A. Jenekhe, Electrospun nanofibers of blends of conjugated polymers: morphology, optical properties, and field-effect transistors. Macromolecules **38** (11), 4705–4711 (2005)
59. N. Pinto, A. Johnson, A. MacDiarmid, C. Mueller, N. Theofylaktos, D. Robinson, F. Miranda, Electrospun polyaniline/polyethylene oxide nanofiber field-effect transistor. Appl. Phys. Lett. **83**(20), 4244–4246 (2003)
60. S. Sharma, M. Madou, A new approach to gas sensing with nanotechnology. Philos. Trans. R. Society A: Math. Phys. Eng. Sci. **370**(1967), 2448–2473 (2012)
61. H. Liu, J. Kameoka, D.A. Czaplewski, H. Craighead, Polymeric nanowire chemical sensor. Nano Lett. **4**(4), 671–675 (2004)
62. A.L. Andrady, *Science and technology of polymer nanofibers* (John Wiley & Sons, New York, NY, 2008)
63. M. Madou, V.H. Perez-Gonzalez, B. Pramanick, *Carbon: The Next Silicon? Book 1—Fundamentals* (Momentum Press, New York, 2016)
64. J.-S. Kim, D.H. Reneker, Polybenzimidazole nanofiber produced by electrospinning. Polym. Eng. Sci. **39**(5), 849–854 (1999)
65. D. Sun, C. Chang, S. Li, L. Lin, Near-field electrospinning. Nano Lett. **6**(4), 839–842 (2006)
66. G. Zheng, G.W. Li, X. Wang, D. Wu, D. Sun, L. Lin, Precision deposition of a nanofibre by near-field electrospinning. J. Phys. D: Appl. Phys. **43**(41), 415501 (2010)

67. C. Chang, K. Limkrailassiri, L. Lin, Continuous near-field electrospinning for large area deposition of orderly nanofiber patterns. Appl. Phys. Lett. **93**(12), 123111 (2008)
68. C.S. Sharma, H. Katepalli, A. Sharma, M. Madou, Fabrication and electrical conductivity of suspended carbon nanofiber arrays. Carbon **49**(5), 173–1727 (2011)
69. J.-I. Heo, Y. Lim, M. Madou, H. Shin, in *Scalable Suspended Carbon Nanowire Meshes as Ultrasensitive Electrochemical Sensing Platforms*. In IEEE 2012 IEEE 25th International Conference on Micro Electro Mechanical Systems (MEMS) (2012), pp. 878–81
70. Y. Lim, J. Heo, M.J. Madou, H. Shin, *Development of Suspended 2D Carbon Nanostructures: Nanowires to Nanomeshes*. The 17th International Conference on Solid-State Sensors, Actuators and Microsystems (Transducers 2013) (2013)
71. J. Heo, Y. Lim, H. Shin, in *A Stacked Electrode Set Including Suspended Carbon Nanomeshes and Planar Carbon Pads for Electrochemical/Bio Sensor Applications*. The 17th International Conference on Solid-State Sensors, Actuators and Microsystems (Transducers 2013) (2013)
72. S. Sharma, in *Microstructural Tuning of Glassy Carbon for Electrical and Electrochemical Sensor Applications*. PhD Thesis, UCI (2013)